INVITED PAPER

# Ge/Si Self-Assembled Quantum Dots and Their Optoelectronic Device Applications

*Integration of optical and electronic devices has been achieved by growth of germanium dots, for photodetectors and LEDs, on silicon substrate.*

By Kang L. Wang, *Fellow IEEE*, Dongho Cha, Jianlin Liu, and Christopher Chen

**ABSTRACT** | In recent years, quantum dots have been successfully grown by self-assembling processes. For optoelectronic device applications, the quantum-dot structures have advantages such as reduced phonon scattering, longer carrier lifetime, and lower detector noise due to low-dimensional confinement effect. Comparing to traditional optoelectronic III-V and other materials, self-assembled Ge quantum dots grown on Si substrates have a potential to be monolithically integrated with advanced Si-based technology. In this paper, we describe the growth of self-assembled, guided Ge quantum dots, and Ge quantum-dot superlattices on Si. For dot growth, issues such as growth conditions and their effects on the dot morphology are reviewed. Then vertical correlation and dot morphology evolution are addressed in relation to the critical thickness of Ge quantum-dot superlattices. In addition, we also discuss the quantum-dot p-i-p photodetectors (QDIPs) and n-i-n photodetectors for mid-infrared applications, and the quantum-dot p-i-n photodetectors for 1.3–1.55 $\mu$m for communications applications. The wavelength of SiGe p-i-p QDIP can be tuned by the size as grown by various patterning methods. Photoresponse is demonstrated for an n-i-n structure in both the mid-infrared and far-infrared wavelength ranges. The p-i-n diodes exhibit low dark current and high quantum efficiency. The characteristics of fabricated light-emitting diode (LED) devices are also discussed, and room-temperature electroluminescence is observed for Ge quantum-dot LED. The results indicate that Ge dot materials are potentially applicable for mid-infrared (8–12 $\mu$m) detectors as well as fiber-optic (1.3–1.55 $\mu$m) communications.

**KEYWORDS** | Infrared detectors; light-emitting diodes; nanotechnology; optoelectronic devices; quantum dots

## I. INTRODUCTION

There have been tremendous efforts in Si-based SiGe microelectronics after successful invention of heteroepitaxial growth, followed by the fabrication of individual devices with high performance [1]–[7]. Due to some unique physical properties of Ge (and/or Si) such as indirect bandgap and comparatively large effective mass [8], the research effort of Si-based photonic components for both mid-infrared and fiber-optic communication wavelengths is much smaller in scale. The primary devices by the use of engineering both interband and intersubband transitions are mostly based on III-V semiconductors like AlGaAs/GaAs and InGaAsP/InP. A clear advantage of investigating Si-based photonics is to integrate optical and electronic devices on a Si substrate by using well-developed Si VLSI technology to achieve low cost. The challenge in the Si-based optoelectronic devices comes from various different features of SiGe heterostructures. Among them, the 4.1% lattice mismatch of Ge and Si as well as the near zero conduction band-offset makes the strategy for both growth and device engineering different from those of III-V compounds.

Ge self-assembled quantum dot (SAQD) grown by molecular beam epitaxy (MBE) and chemical vapor deposition (CVD) is one of promising candidates to achieve the deposition of pure Ge without the presence of a large

Manuscript received March 7, 2007; revised April 30, 2007. This work was supported in part by the MURI program supported by Army Research Office (Dr. William Clark) and in part by the FCRP Focus Center on Functional Engineered Nano Architectonics—FENA (under Dr. Betsy Weitzman).

**K. L. Wang** and **D. Cha** are with the Department of Electrical Engineering, University of California at Los Angeles, Los Angeles, CA 90095 USA (e-mail: wang@ee.ucla.edu; dhcha@ee.ucla.edu).

**J. Liu** is with the Department of Electrical Engineering, University of California at Riverside, Riverside, CA 92521 USA (e-mail: jianlin@ee.ucr.edu).

**C. Chen** was with the Department of Electrical Engineering, University of California at Los Angeles, Los Angeles, CA 90095 USA. He is now with Altera Corporation, San Jose, CA 95134 USA (e-mail: chrchen@altera.com).

Digital Object Identifier: 10.1109/JPROC.2007.900971



0018-9219/$25.00 ©2007 IEEE

density of dislocations, leading to lower leakage current. Multilayer Ge dots interlaced with thin Si layers can then be grown for increasing the quantum efficiency. The ability of self-assembled Ge quantum dots by the Stranski–Krastanov (SK) method to form the energy-quantized islands without any artificial masking and patterning as well as their compatibility with the current Si technology provides potentials for the fabrication of novel devices on Si [9]–[11]. On the other hand, the long-standing issues of Ge SAQD on Si, such as size control and exact placement of dots, have been the problems. More recently, these problems are resolved by guided growth, usually selective epitaxial growth on patterned mesas or patterned holes with nanometer-scale width, depth, and period [12]–[16]. By the use of these patterning-assisted quantum dots (PAQDs) with uniform size and placement, high density has been achieved on Si.

Ge/Si quantum dots exhibit a type-II band lineup [17]. The large valence band offset leads to an effective confinement of holes in the Ge region while electrons are mostly presented in the Si layers. In case of interband transition, one has to change the dot size or Ge mole fraction in dots to tune the photoresponse to the desirable spectral region, like around 1.55 $\mu$m. The Ge/Si SAQD system may also have potential applications for fabricating on-chip light-emitting sources. There were some theoretical results on an indirect-to-direct conversion of the optical transition of SiGe quantum dots due to small enough size of the quantum dots [18], [19]. Photoluminescence studies have been carried out extensively on the Ge/Si quantum dots [20]–[25], and the electroluminescence of Ge quantum dots was observed up to room temperature in the spectral region around 1.3–1.5 $\mu$m [26].

In this paper, we mainly deal with the fabrication of Ge SAQDs, PAQDs, and multilayered quantum dots (MLQD) on Si (100), their optoelectronic properties, and related optoelectronic devices. First, the growth of Ge quantum dots and the corresponding formation mechanism will be discussed. Then, the results of near-infrared properties of Ge quantum dots by photoluminescence studies will be described, followed by the description of mid-infrared properties of boron-doped Ge quantum dot and phosphorus $\delta$-doped Ge quantum dot. Finally, optoelectronic devices based on Ge quantum dots are reported.

## II. SELF-ASSEMBLED AND GUIDED Ge QUANTUM DOTS

In heteroepitaxial growth, there are generally three growth modes: namely, the Frank van der Merwe (FM), the Volmer–Weber (VW) and the SK growth modes [27]. They can be described as layer-by-layer growth, island growth, and layer-plus-island growth, respectively. Ge films grown on Si follow the SK growth mode. The dot formation via the SK mode uses the transition from the 2-D layer growth to 3-D island growth. A lattice constant mismatch between the Si and Ge atoms is a key driving force for the dot formation. At the beginning of the growth of Ge on Si, misfit strain is built up and fully accommodated. Once the Ge film thickness exceeds its critical thickness of a few monolayers, the strain starts to relax, small pyramidal islands are formed, and the film morphology becomes rough. Those small islands may evolve to large domes after more Ge is deposited. When Ge deposition exceeds 2 nm, misfit dislocations and threading dislocations form to relieve the additional strain arising from the accumulation of the film thickness [28]. This strain-related self-assembled dot formation offers the possibility to fabricate islands with uniform size without any substrate patterning process.

Fig. 1 shows a 2-D AFM image of Ge SAQDs on Si (100) substrate. Ge dots were grown at 550 °C by MBE [29]. The growth method employed in this study is MBE unless specified otherwise. The nominal Ge thickness is 1.7 nm. Two kinds of Ge dots are shown. The larger dots are multifaceted domes (A) and the smaller dots are square-based pyramids (B). They have a distinct shape and a distinguishable size distribution. They are referred to as a *bi*-modal distribution [30]. A *bi*-modal distribution of Ge dots is a typical experimental result for Ge/Si (100).

Based on kinetic and thermodynamic analyses, there are two basic interpretations for the experimental observations. In real-time low-energy electron microscopy, Ross *et al.* [31] studied the evolution of Ge SAQDs and

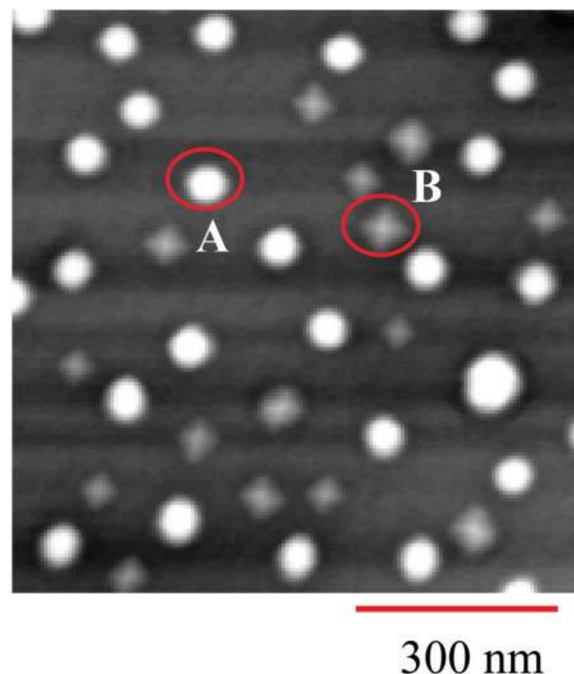


**Fig. 1.** *2-D AFM image of typical bi-modal Ge dots: (A) multifaceted domes and (B) square-based pyramids [29].*

found that the size of large dots increased at the expense of small dots and concluded that it was a kinetic process driven by an Ostwald ripening effect. Based on thermodynamic analysis, Shchukin *et al.* [32] proposed that for some systems, there are minima in the free energy of self-assembled dot ensembles showing the size with a stable Boltzmann distribution. Kamins *et al.* [33] conducted annealing experiments to distinguish the stages of the two mechanisms, Ostwald ripening and equilibrium distribution. They found that dot evolution was slowed with increasing annealing time at 550 °C and 600 °C. It would finally reach an equilibrium distribution.

For many potential applications, the control of the dot size distribution is one essential issue. A narrow distribution or high uniformity is desirable. A *bi*-modal or *multi*-modal distributions of dots in Ge/Si (100) system are obstacles for accomplishing a uniform size of dots. The uniformity of dots has been found to depend critically on the growth parameters, such as growth temperature, growth rates, Ge deposited coverage, and holding time at the growth temperature after Ge deposition. Uniform *mono*-modal quantum dots can be obtained by properly controlling these growth conditions. The study of the growth temperature influence on the formation of the self-assembled Ge dots on Si (001) substrates was reported. For the Ge growth rate of 0.2 Å/s and the Ge coverage of 1.5 nm, the growth temperature for achieving a high uniformity in the dot size was found to be around 600 °C. Fig. 2(a) shows a 2-D AFM image of the highly uniform Ge dots on Si (100) substrate at a growth temperature of 600 °C [34]. Fig. 2(b) is the composed 3-D view. The dots are all dome-shaped with the base size and the height of about 70 nm and 15 nm, respectively. The areal density of the dots is about $3 \times 10^9$ cm$^{-2}$ and the height deviation of the dots is about ±3%. This result demonstrates the possibility of uniform Ge dots on Si

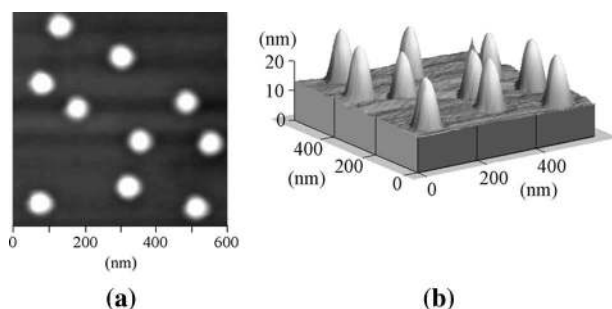


**Fig. 2.** ***(a) 2-D AFM image of the uniform self-organized Ge dots on Si (0 0 1) at the growth temperature of 600 °C. The Ge thickness is about 1.5 nm. The base size and the height of the dots are about 70 nm and 15 nm, respectively, and the height uniformity of the dots is about ±3%. The areal density of the dots is about $3 \times 10^9$ cm$^{-2}$. (b) The corresponding 3-D AFM image [34].***

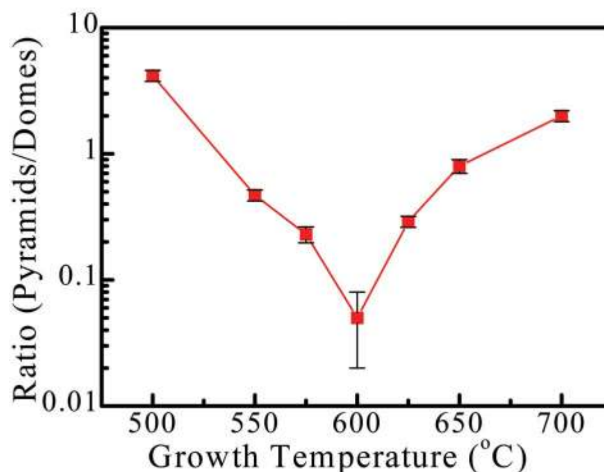


**Fig. 3.** ***The number ratio of pyramids to domes versus growth temperature. The optimum temperature is about 600 °C for the formation of mono-modal morphology dots. Note that the at high temperature, small dots occur in the precursor state are not counted [29].***

(100). The possible mechanism associated with the highly uniform distribution was attributed to the enhanced diffusion [35].

Fig. 3 plots the number ratio of the pyramids to the domes versus the growth temperature as reported in [29]. It is interesting to find a nearly symmetric behavior with the center temperature at 600 °C. As the temperature increases from 500 °C, the ratio of the *bi*-modal dots reduces and reaches a minimal value at about 600 °C, and then increases again beyond this temperature. The optimum growth temperature for the formation of the *mono*-modal distribution of the Ge dots occurs at 600 °C. The formation of the *mono*-modal distribution was attributed to the enhanced diffusion kinetics at higher growth temperatures. The dot size increases as the temperature increases, leading to the accommodation of larger strain in the dots, especially around the dot edges. On the other hand, the intermixing may occur and becomes pronounced as the temperature increases beyond 650 °C [36], which results in the modification of the interface strain distribution, and thus leads to the reoccurrence of *bi*-modal dots. Due to the intermixing of Si with Ge, the wetting layer is no longer a pure Ge layer, but a SiGe-like layer, and then the lattice mismatch becomes smaller than 4.1%, and the strain energy is thus reduced leading to the larger pyramids at higher temperatures [37]. Meanwhile, the relaxation of the strain around the edges will cause dislocations to develop, which increase the intermixing by lowering the intermixing barrier. However, at lower temperatures ($\leq$ 550 °C), the diffusion is limited and impedes the formation of uniform dots.

In order to clarify the dependence of dot density on temperature, the values of the average dot spacing (also

called the characteristic length) $L_c$, which was defined as the inverse of the square root of the areal density $\sigma$, were calculated from the experimental results. Fig. 4 plots the Arrhenius relation of the average dot spacing $L_c$ versus growth temperature [29]. It is found that a discontinuity of $L_c$ occurs at the temperature of 600 °C with two slightly different slopes, corresponding to the activation energies of 0.88 eV and 0.91 eV, respectively. These suggest that diffusion is not the only driving force for determining the dot density at higher temperatures. Intermixing of Si with Ge taking place at the temperature of above 600 °C [38], [39] may also be responsible for the observed discontinuity. The change of activation energy also indicates the change of the mechanism from enhanced diffusion at lower temperatures to the intermixing of Si with Ge at higher temperatures investigated.

For electronic and signal processing applications, controlled spatial arrangement is usually required. In order to control spatial distribution, much effort has been devoted using a variety of techniques, such as growth on miscut substrates with surface steps [40] and on relaxed templates with dislocation networks [41], [42] and stacking growth of multilayers of dots [43], [44]. One of the most effective approaches is using selective epitaxial growth (SEG) mesas as templates for subsequent Ge growth [34]. Fig. 5(a) shows a 3-D AFM image of self organized Ge dots on the ⟨110⟩ oriented Si stripe mesas, formed on the exposed Si stripe windows with a window width of 0.6 $\mu$m and a separation between two stripes of 0.1 $\mu$m. Perfectly aligned and regularly spaced 1-D arrays of the Ge dots are formed on the ridges of the Si stripe mesas. This almost perfect alignment of the dots along the Si stripe mesas is due to the formation of the ridges, which results from the full reduction of the top surface of the stripe mesas. Fig. 5(b) depicts the 2-D image of the dot arrays in Fig. 5(a). The cross-sectional profile of the mesas and an array of the dots are shown in Fig. 5(c). The average sizes of the Ge dots are about 80 nm wide and 20 nm high, and the period is about 120 nm. The regimented arrangement is the result of cooperative interaction from the neighboring dots caused by the balance of diffusion, the strain energy, and the repulsive interaction among the dots. The repulsive interaction comes from the elastic tensile deformation of the substrate by the dots [45], [46].

The patterned substrates can be used for fabricating quantum dots (PAQD) with uniform size and placement, and high density. One method to get these nanopatterned substrates as a template is to use a self-assembled diblock

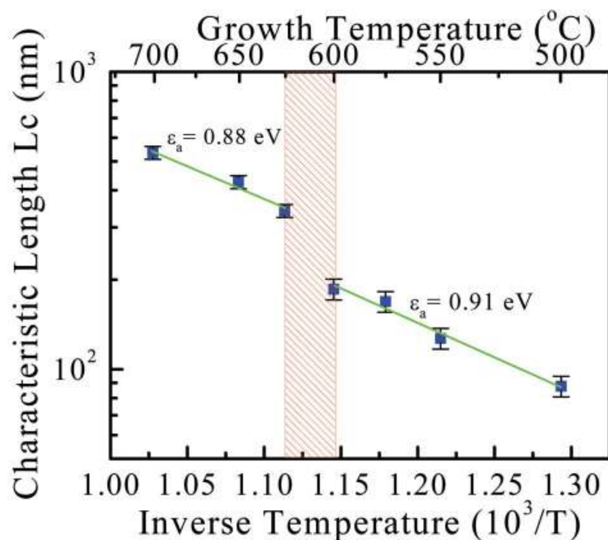


**Fig. 4.** ***The characteristic length ($L_c$) versus the temperature, where the square of the length ($L_c^2$) is defined as inverse areal dot density. Note that the $y$-coordination is in a logarithmic scale to clarify the Arrhenius relation [29].***

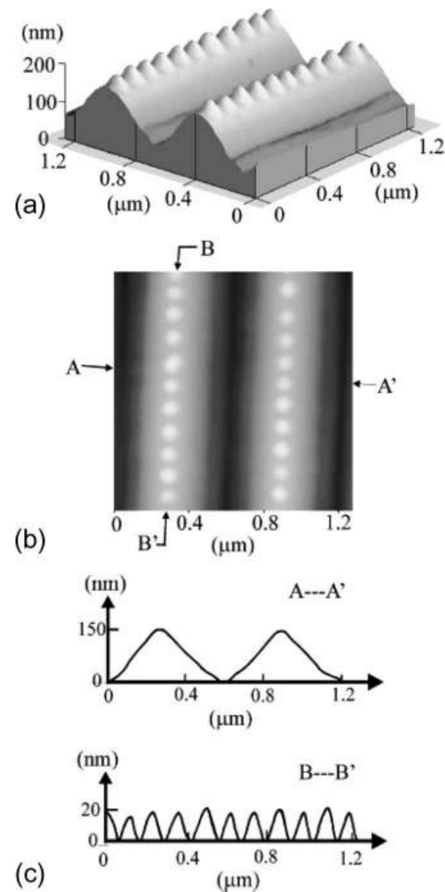


**Fig. 5.** ***(a) A 3-D AFM image of the self-assembled Ge dots on the ⟨110⟩ oriented Si stripe mesas with a window width of 0.6 $\mu$m. Self-aligned and well-spaced 1-D arrays of the Ge dots are formed on the ridges of the Si mesas after the deposition of 10 ML Ge. (b) The 2-D image of the dot arrays in (a). (c) The cross sections of the mesas (line AA′) and one array of the dots (line BB′), respectively [34].***

copolymer [47], [48]. Here, we show Ge quantum-dot growth in nanopatterns on Si (100) substrate by solid-source MBE [49]. Si substrates with hexagonally ordered hole patterns on the surface are prepared using a self-assembled diblock copolymer. Typical diblock copolymer used in our work is polystyrene-block-poly(methylmethacrylate) (PS-b-PMMA) [50], [51]. The process is described in Fig. 6(a). A 30 nm layer of $SiO_2$ is deposited on the wafer by low-pressure chemical vapor deposition (LPCVD). Then, a 30 nm layer of PS-b-PMMA is spin-coated on top of the $SiO_2$. With an annealing at 170 °C in vacuum, PMMA become spatially separated from PS in a hexagonal close-packed configuration. After exposure to ultraviolet (UV) for 35 min, the PS is cross-linked and the PMMA is separated. After rinsing in acetic acid, cylindrical pores are produced in the PS matrix. By a $CHF_3$ dry etch, the hexagonally organized cylindrical pattern of PS-b-PMMA on the top layer is transferred to the underlying $SiO_2$ layer forming hole patterns with a diameter of, e.g., ~30 nm, a center-to-center distance of ~40 nm, a depth of ~20 nm, and a density of ~$10^{11}$ $cm^{-2}$. The growth conditions are chosen to be selective in the patterned holes. The typical growth rates of Si and Ge are 0.4 and 0.25 Å/s, respectively. To ensure desorption of GeO and SiO, the growth temperatures are kept at 620 °C for Si and 530 °C for Ge layers. Fig. 6(b) is a plan-view SEM image of the Ge dots with the $SiO_2$ mask etched away. The Ge dots are grown at 530 °C with a 4 nm coverage.

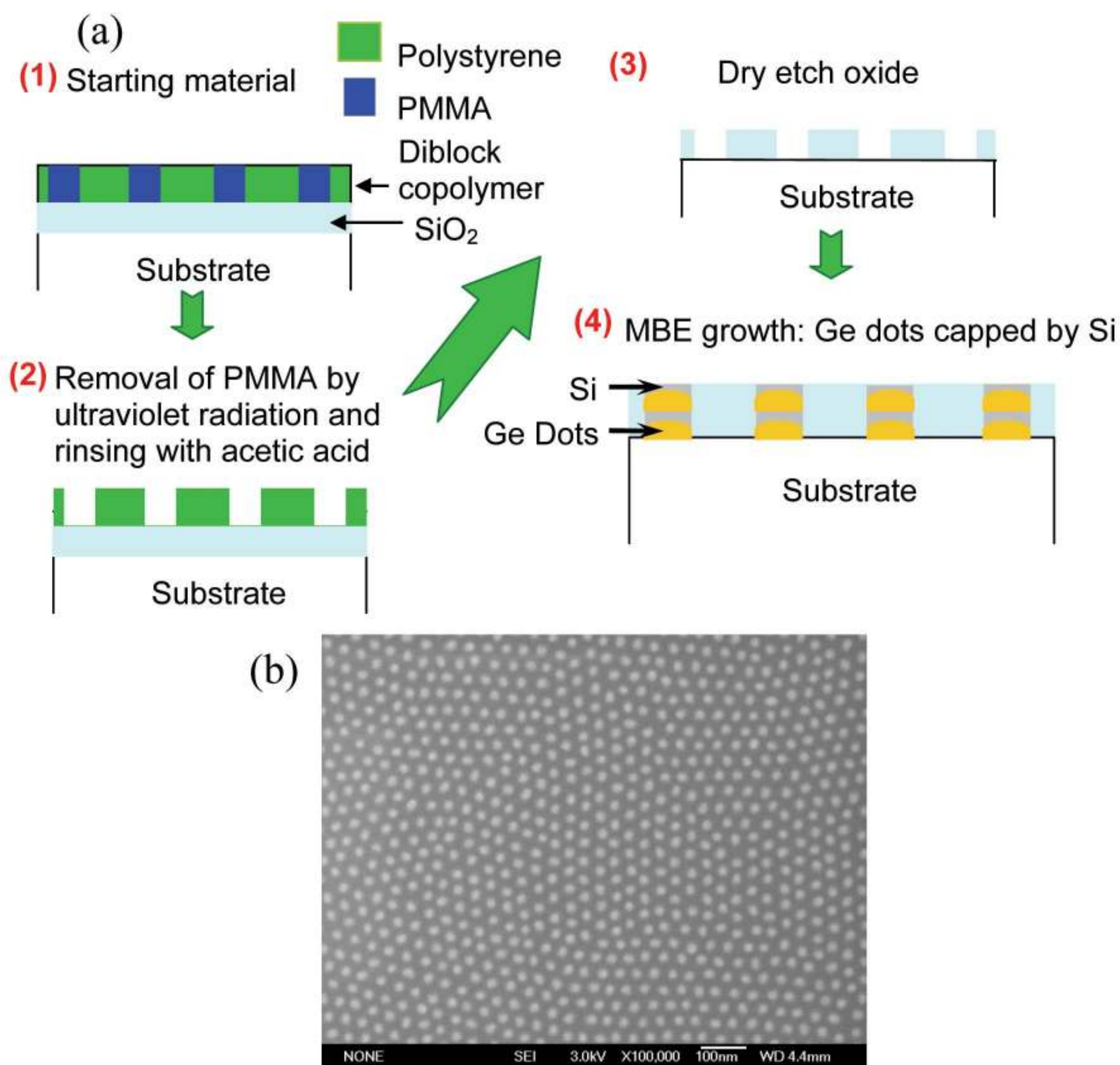


**Fig. 6.** *(a) Ge PAQD growth on the nanopattern. (1) PMMA separated from PS in regularly spaced hexagonal-close-packed arrangement. (2) Removal of PMMA by ultraviolet radiation and rinsing in acetic acid. (3) Dry etch of oxide in $CHF_3$ plasma. (4) MBE growth of Ge PAQD capped by Si. The dots are selectively grown on Si substrate. (b) Plan-view SEM image of Ge PAQDs with the $SiO_2$ mask etched away. Dots are grown at 530 °C with a 4 nm coverage. It shows hexagonally ordered small Ge quantum dots with an average height of ~5 nm, a lateral size of ~30 nm, and a high density of ~$10^{11}$ $cm^{-2}$.*

The hole-patterns provide the preferential nucleation sites for the Ge dots. The Ge PAQDs have an average height of ~5 nm and a lateral size of ~30 nm. It also shows a high density of ~$10^{11}$ $cm^{-2}$ and a high ordering with hexagonal symmetry. These pattern qualities could not be easily achieved using planar nonpatterned substrates. These results show that the use of the template growth is an important alternative approach to obtain dots for device applications, such as IR, diode, lasers, and single-electron devices. The approach of using a self-assembled diblock copolymer to achieve nanopatterns on Si substrates for ordered Ge quantum dots holds a high promise.

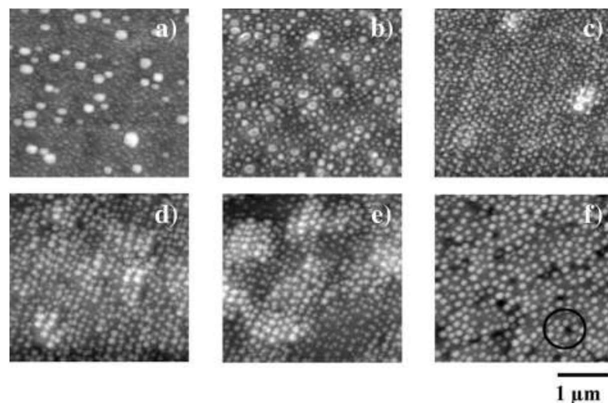


**Fig. 8.** ***AFM images of Si (20 nm)/Ge (1.5 nm) multilayers having (a) 2, (b) 5, (c) 10, (d) 20, (e) 35, and (f) 50 periods. The increasing uniformity is clearly observed as the period increases (< 35 periods). The surface under the dot layer for the 50-period sample exhibits clearly some circular holes with one of them decorated by a circle, which are induced by threading dislocations. The dots near to these holes tend to nucleate near the edges. The samples are grown at 540 °C by the SK growth mode.***

## III. MULTILAYERED Ge QUANTUM DOTS (Ge MLQD)

For some applications such as optoelectronics, multilayered Ge quantum-dot superlattices are very important. An interesting feature observed in the multilayered structures is vertical correlation during deposition of Ge/Si multilayer structures. The origin of the vertical correlation may be attributed to preferential nucleation due to an inhomogeneous strain field induced by buried dots [52]. The Si cap layers are tensilely strained above the buried Ge dots, but the surface is usually not flat after the Si cap layer growth, even if the Si capping layer thickness exceeds the island height. The surface roughness is strongly correlated with the mechanism of the vertical alignment of Ge islands on Si for a multilayer structure. In many publications, the evolutions of the dot size, the size distribution, and the density of dots in the Ge dot multilayers have been observed [52], [53]. Here, we report the morphology of Ge dots and misfit dislocations as a function of the number of multilayers.

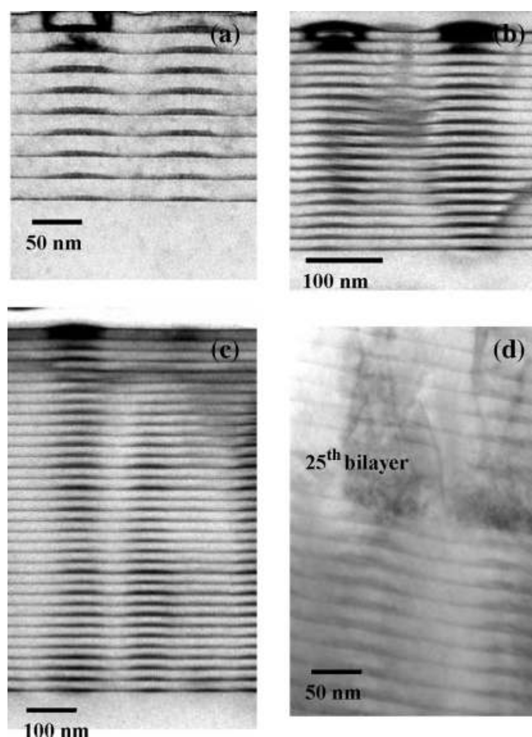


**Fig. 7.** ***Cross-sectional TEM images of (a) 10, (b) 20, (c) 35, and (d) 50-period Si (20 nm)/Ge (1.5 nm) superlattice samples. Vertically correlated dots are observed for all four samples, but the high-density of dislocations is evident for the 50-period sample. The samples are grown at 540 °C by the SK growth mode.***

Fig. 7 shows the cross-sectional TEM images of samples. The difference of the samples was the multilayer period. The samples were grown at 540 °C by the SK growth mode having the Ge and Si nominal thicknesses of 1.5 and 20 nm in each period, respectively. Coherent vertical-correlated Ge dots were observed for all four samples. But, a high-density dislocation was generated when the film reached the 25th period for the 50 period sample. The dislocations penetrated to the subsequent layers on top. Fig. 8 shows the AFM images of the top surfaces of the Ge quantum-dot superlattice samples with different periods of 2, 5, 10, 20, 35, and 50. For the samples with fewer than 35 periods, the size uniformity of Ge quantum dots increases with an increasing number of periods. The surface under the dot layer is relatively flat. For the sample having 50 periods, the surface under the dot layer shows some circular holes induced by threading dislocations. Fig. 9 shows the Ge dot density and the root-mean-square (rms) dot height relative to the average dot height ($\langle \Delta H \rangle / \langle H \rangle$ indicates nonuniformity) as a function of the number of periods. The density of dots decreases dramatically as the period increases and saturates at ~$2 \times 10^9$ $cm^{-2}$ when the period exceeds 20.

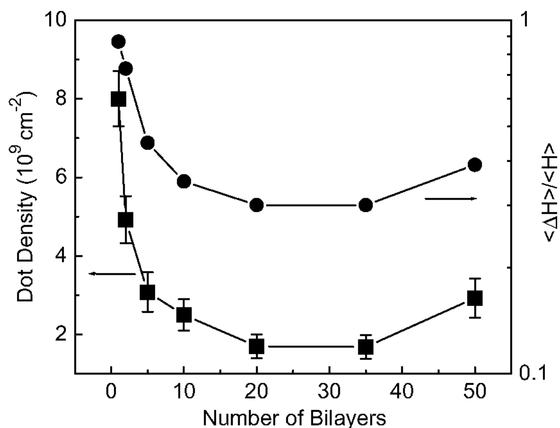


**Fig. 9.** ***Ge quantum-dot density and rms height relative to average height as a function of the period for Si (20 nm)/Ge (1.5 nm) multilayers. The dot density decreases dramatically as the period increases and saturates at about $2 \times 10^9$ cm$^{-2}$ when the period reaches 20. After 35 periods, the density increases slightly, indicating the change of growth mode or the generation of threading dislocations in the samples. The increasing uniformity with the multilayer period fewer than 35 is observed. After the first 35 periods, the uniformity becomes worse. The trend of the data for both the density and the height of dots suggests the change of growth mode or the generation of threading dislocations in the thick samples.***

After 35 periods, the density increases slightly, indicating the change of growth mode or the generation of threading dislocations in the samples. The increasing uniformity with the multilayer period fewer than 35 is evident. It comes from the increasing uniformity of the strain distribution in the upper layers as predicted by the elastic continuum model [54]. For samples having greater than 35 periods, the uniformity becomes worse, showing a very high density of threading dislocations due to strain relaxation.

The strain-related vertical correlation is related to spacer layer thickness. The strain field from the underlying coherent dots can penetrate through the thin Si spacer layers. When the spacer layer becomes thicker than a critical value, the random arrangement of Ge dots is resulted. Therefore, the Si spacer layer thickness is the key factor to keep vertical correlation and can influence the distribution of the misfit strain on the surface. Rahmati *et al.* [55] found that the strain field from the buried islands was too weak to induce vertical correlation when the Si spacer layer thickness was greater than 100 nm. Kienzle *et al.* [56] examined the vertical correlation of Ge dots as a function of Si spacer layer thickness. They found the increase of the average island size with increasing the number of layers. There seems to have a transition regime from the perfect correlation to random arrangement as the thickness of the Si spacer layer increases from 30 to 100 nm. Tersoff *et al.* [54] examined the influence of the areal density of the initial Ge dot layer on the subsequent Ge dot layers, and calculated that the areal density of the subsequent Ge dot layer also varied with the Si spacing layer thickness.

## IV. INTERBAND AND INTERSUBBAND PROPERTIES

For near-infrared optoelectronic applications, it is very important to understand interband optical properties. Fig. 10 shows a low-temperature photoluminescence (PL) spectrum at 4.2 K of the Ge quantum-dot superlattice with a Ge dot height of 12 nm and a base diameter of 110 nm. This sample contains ten periods of Ge/Si (20 nm) layers. It was grown at the temperature of 540 °C. The peaks at 1.153, 1.132, 1.095, 1.061, and 1.027 eV are presumably originated from Si and they correspond to nonphonon (NP) replica, transverse acoustic (TA), transverse optical (TO), 2TA + TO, and TO + $O_\Gamma$ peaks, respectively. The broad peak with the peak energy at 0.963 eV is attributed to the Ge wetting-layer. The peak at 0.771 eV is from the Ge quantum dots. The inset shows the possible mechanism for the NP peak arising from the Ge quantum dots. The Ge/Si multilayer structure has a type-II band alignment. Radiative recombination occurs between electrons in the Si layers and holes confined in the Ge dots, giving rise to the Ge quantum-dot peak in the PL spectrum. To the first-order estimation, the energy of the ground state mainly stems from the vertical quantum confinement due to the height of the dots. The lateral sizes of our dots are more than 110 nm, a value that is too large to induce lateral confinement.

The PL spectra of three samples with different Ge coverages are shown in Fig. 11. Each sample contains ten periods of Ge/Si (20 nm) layers. These samples were grown

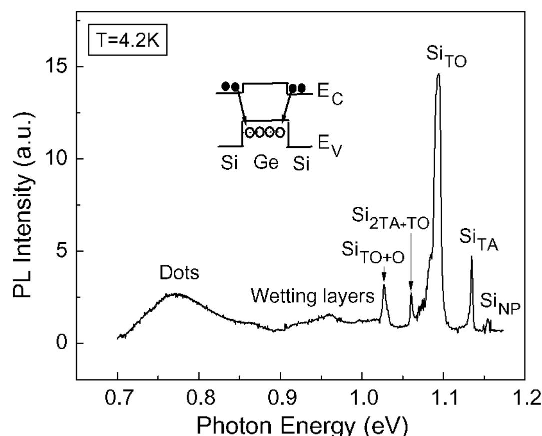


**Fig. 10.** ***Typical low-temperature PL spectrum of a 10-period Ge quantum-dot film at 4.2 K. The inset shows the mechanism of the emission of the quantum-dot peak at 0.771 eV.***

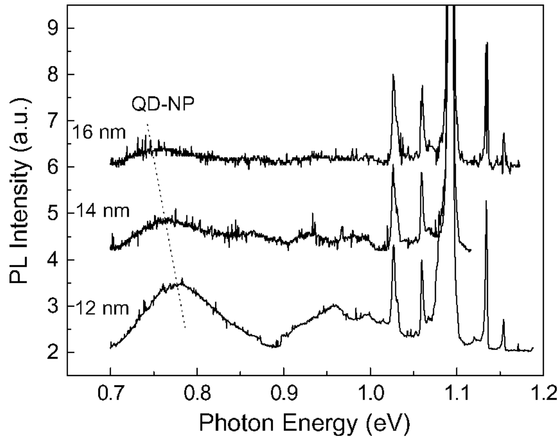


**Fig. 11.** ***PL spectra at 4.2 K for a series of samples with different dot heights of 12, 14, and 16 nm. As the dot size increases, the quantum-dot NP peak shifts to the low-energy side. The energy shifts by about 28 meV for the dot height changing from 12 to 16 nm.***

on Si (100) substrates at 540 °C. AFM measurements indicate that the dot heights are 12, 14, and 16 nm, while the dot base diameters are 110, 122, and 122 nm, respectively. As the dot height increases from 12 to 16 nm, the NP peak of the quantum dots shifts by 28 meV to the low energy along with a decrease in the integrated peak intensity under each dot peak. The latter fact further supports the argument in favor of the type-II band alignment for the Si/Ge dot system; the holes and electrons are separated in the Ge and Si in a type-II structure, respectively (shown in Fig. 10, inset). As the dot size decreases, the energy increases, and the hole wave function penetrates more into the Si layer; likewise, the electron wave also penetrates into the Ge dot. As a result, the oscillation strength becomes larger with the overlap of these wave functions.

Fig. 12(a) shows the PL results for samples with the different numbers of periods. Each period consists of Si (20 nm)/Ge (15 nm). Fig. 12(b) gives the quantitative summary of the quantum-dot peak energy as a function of the number of periods. The effect of the period on the quantum-dot peak is obvious. As the period increases to about ten, the peak energy decreases first and then increases. This is because before the first ten periods, the coarsening effect plays an important role and the average dot size increases. Therefore, the dot peak shows a red shift. After the tenth period, there is no significant change in the dot size. The increase of the peak energy with the number of the period is presumably due to the strain relaxation of the dots. This can be seen from the spectra that starting from the 20-period sample, the dislocation related peak, D2, at around 0.86 eV appears. The strain relaxation becomes larger as the number of periods increases. Therefore, the ground state of quantum dots decreases, leading to the blue shift of the quantum-dot peak. The integrated PL intensity of the quantum-dot peak increases as the number of periods increases to 35, then suddenly decreases afterwards. In this case, due to the strain relaxation, threading dislocations appeared to degrade PL.

Intersubband transition in quantum confined semiconductor nanostructures is a subject of interest both for fundamental physics as well as for the development of infrared photodetectors and sources in the mid-infrared region. Self-assembled quantum dots (SAQDs) based on the SK growth mode are pancake-like dots with relatively large base dimensions of 50–100 nm, short heights of 7–10 nm, and a low areal dot density of $10^9 - 10^{10}$ cm$^{-2}$. Such SAQDs have poor lateral confinement, and thus does not have normal-incidence absorption characteristics, similar to the quantum well case.

We have demonstrated infrared absorption in Ge PAQDs grown on nanopatterned substrates. The process has been described in the previous sections. In order to achieve infrared absorption between two valence band substrates, the dots are doped with boron to a concentration

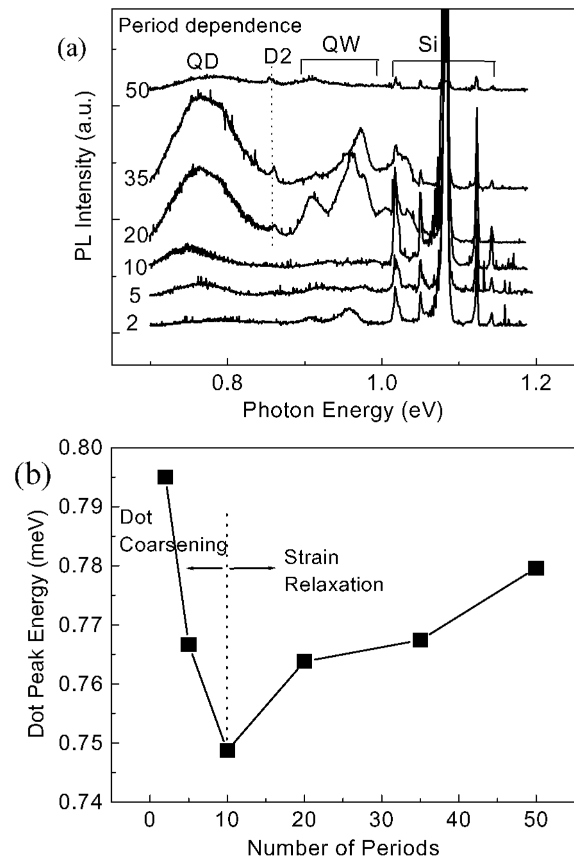


**Fig. 12.** ***(a) PL spectra of multilayered Ge quantum-dot samples with different periods (2–50). (b) The plot of quantum-dot peak energy versus the number of periods from (a).***

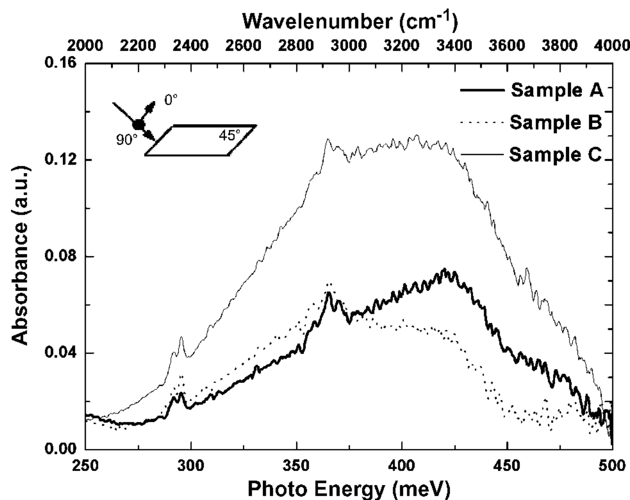


**Fig. 13.** ***FTIR absorption spectra for samples A, B, and C (A: Ge dots with 15 nm base and 7 nm height, B: $Si_{0.5}Ge_{0.5}$ dots with the 15 nm base and the 7 nm height, C: 15 nm base and 5 nm height). For the spectra, the background spectra have been subtracted. The polarization angle is defined in the inset. Here, the 90° polarization angle means that the electric field of the incident light is parallel to the surface of the sample, along the layer (or perpendicular to the growth direction), while the 0° polarization angle is that the electric field makes a 45° angle with the growth direction [49].***

of $10^{20}$ cm$^{-3}$. The nominal $Si_{1-X}Ge_X$ deposition thickness is 7 nm for samples A and B and 5 nm for sample C; the Ge content is $x = 0.5$ for sample B or $Si_{0.5}Ge_{0.5}$, while $x = 1$ for the other two.

Fig. 13 shows the measured absorption spectra of samples A, B, and C at the 0° polarization angle. Absorption peaks are found near 3380 cm$^{-1}$ (3.0 $\mu$m) and 2900 cm$^{-1}$ (3.5 $\mu$m) for sample A and B, respectively. The peaks are attributed to intersubband transitions in the Ge quantum dots. Due to the reduced valence-band offset with decreasing $x$ and reduced subband energy differences with decreasing Ge fraction ($x$) [57], [58], sample B has a longer wavelength transition between the ground state and the continuum band edge. For sample C, an absorption peak is found near 3.1 $\mu$m. The shift in the intersubband absorption peak for sample C is due to the small size of Ge dots in the sample (5 nm in height). As the dimension of the quantum dots decreases, the ground state energy of the system increases. Therefore, a transition between the increased ground state and the continuum band edge induces a red shift in the absorption spectra for sample C.

Fig. 14(a) shows the polarization dependence of sample A. A similar result is obtained for sample C. The absorption reaches the maximum at the 0° polarization angle and decreases with increasing polarization angle. Sample A still shows a significant absorption even at the 90° polarization angle. These results show that sample A exhibits normal incidence absorption. Since the effective mass of the heavy hole is larger than that of the light hole, we expect a heavy hole ground state in the valence band. The transition matrix elements from the heavy hole ground state to an light hole state may not vanish for normal incident light [59]. If the quantum dots are sufficiently small, this normal incidence absorption may also arise from the quantum confinement of a finite lateral dimension. Since, the average lateral size of our samples is 15 nm, a significant normal absorption may come from a stronger quantum confinement of the small lateral size.

The measured polarization dependent absorption spectra of sample B at the 0° and 90° polarization angles are shown in Fig. 14(b). It is interesting to note that the absorption at the 90° polarization angle is similar of that at the 0° polarization angle. Such strong normal incidence absorption of sample B may be explained by an eight-band $k \cdot p$ theory [60]. The momentum matrix consists of the band-edge Bloch part and the envelope wave function part.

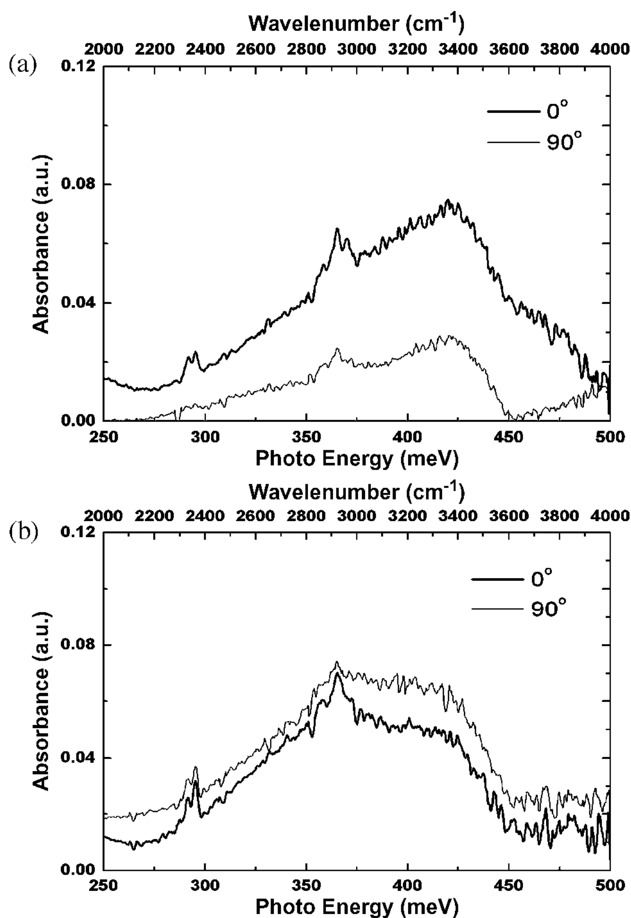


**Fig. 14.** ***(a) Polarization dependent absorption spectra of sample A (Ge dots with 15 nm base and 7 nm height). (b) Polarization dependent absorption spectra of sample B ($Si_{0.5}Ge_{0.5}$ dots with 15 nm base and 7 nm height) [49].***

For the angular incidence case, the band-edge Bloch part dominates, while the envelope wave function part also has a significant contribution for the normal incidence case, different from the quantum well case. This difference may come from the shape and strain of quantum dots. The dominant part also depends on the Ge content according to the theoretical work. For example, for low Ge, the two parts are comparable in magnitude and thus normal incidence detection can be significant. It is also possible, however, that the transitions of the heavy hole to the light hole substates contribute to the absorption and thus detection.

## V. OPTOELECTRONIC DEVICE APPLICATIONS

The 3-D confinement provided by quantum dots allows for special electrical and optical properties. Quantum-dot system offers a great potential in photonic and electronic applications. Furthermore, the growth of Ge dots on Si substrates offers the potential for integration with existing CMOS platforms. For different applications, different requirements are needed. For quantum-dot infrared photodetector (QDIP), high density and very uniform dot size are the critical factors. For light-emitting diodes (LEDs) and perhaps laser application eventually, low defect density and high size uniformity are the most important requirements. The precise control of dot size, shape, and site are the most important for nanoelectronics applications such as single-electron devices. Here, we describe two kinds of applications of Ge quantum dots: Ge QDIP and Ge LED.

QDIP is a promising candidate to rival the current HgCdTe detectors in mid-infrared applications. Quantum dots have several advantages over conventional quantum wells for this application. One is that it has the selective rule to enable normal incidence photon detection when the lateral size is further reduced, which makes the design of the detector structure much easier compared with the quantum well infrared photodetector (QWIP) [61]. Another important advantage is that it has low dark current, higher detectivity, and responses at elevated temperatures, due to reduced carrier-phonon interactions in the quantum-dot system, which leads a predicted long carrier lifetime in excited states [62].

LEDs might be possible using multilayered Ge dot superlattices. The superlattices can be used as a gain media in which interband transitions in indirect semiconductors like Si and Ge occurs as assisted by phonons. Using quantum-dot superlattices, the phonon dispersion can be changed by quantum confinement and the phonon group velocity can be controlled, leading to "phonon engineering" of the structure. Thus, the dot superlattice can be used as a phonon filter when both quantum-dot size and a distance between dots are comparable with the phonon wavelength.

## VI. MID-INFRARED Ge QUANTUM DOT p-i-p PHOTODETECTORS

For the last decade, much progress has been made in the fabrication of the Ge quantum-dot mid-infrared photodetectors [63]–[66]. These detectors are basically consisted of a photoconductor with an active region, which consists of doped semiconductor quantum dots. Under infrared excitation, carriers are photoexcited via intersubband absorption and give rise to the photocurrent.

The Mid-infrared diode structure was fabricated on double-side-polished Si (100) wafers with a boron doping density of $1 \times 10^{19}$ $cm^{-3}$ (Fig. 15). The active region was embedded between two $P^+$ Si layers (200 nm) with a Si (100 nm) intrinsic spacer on each side. The active region consists of 20-period of boron-doped Ge quantum-dot layers separated by 20 or 50 nm Si barriers. Different doping levels from 0.6 to $6 \times 10^{18}$ $cm^{-3}$ for Ge layers were used. The nominal Ge deposition thickness was 1.5 nm. The growth rates for Si and Ge were 0.2 and 0.025 nm/sec, respectively. The growth temperature was kept at 540, 600 and 700 °C during the growth for different samples. Mesas of the size of $250 \times 250$ $\mu m^2$ and $500 \times 500$ $\mu m^2$ were processed by standard photolithography. Ti/Al ohmic contacts were formed by 1 min annealing at 400 °C by RTP. *I–V* measurements were carried out with a HP4145 semiconductor parameter analyzer. The photocurrent was measured in the normal incident configuration with a monochromator and a lock-in amplifier.

Fig. 16(a) shows the *I–V* curves of three samples, A, B, and C at 77 K. The Si spacers has a thickness of 20, 20, and 50 nm and the Ge doping levels of $6 \times 10^{18}$ $cm^{-3}$, $0.6 \times 10^{18}$ $cm^{-3}$, and $6 \times 10^{18}$ $cm^{-3}$, respectively for sample A, B, and C [67]. Nonsymmetric *I–V* curves for the reverse and forward biases are due to the growth direction, for both the wetting layer and the dot shape. Comparing the results for A and C, one can see that by increasing spacer layer thickness, the dark current

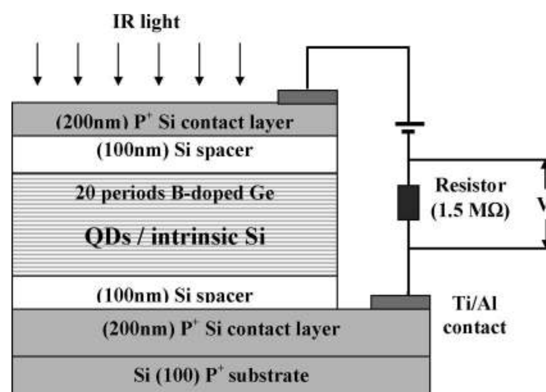


**Fig. 15.** *Schematic drawing of a mesa-type Ge QD photodetector. The active layer consists of 20 periods of boron-doped Ge QD layers separated by 20 nm Si barriers.*

decreases. This is mainly due to the reducing of the electrical field. The difference of the current is about 2.5 times for +1 V and 5.7 times for −1 V. Comparing A and B, one can see that by increasing the doping level 10 times, the dark current increases by 4–5 orders of magnitude. This is in part due to the use of a higher carrier density. In addition, the Fermi level increases by doping. A higher doping level causes carriers to fill the dot to a higher energy, so that the Fermi level is elevated (or downward in the valence sublevel) [Fig. 16(b)].

Fig. 17 shows the normal incidence photoresponse spectra of the sample grown at 700 °C at different measurement temperature. The device has a response in the range of 2.8–4.8 $\mu$m, with the peak at around 3.5 $\mu$m. This response is due to the hole absorption of photons between the valence subbands of the Ge dots. Once the holes in the Ge dots are excited to the band edge, they are swept by the applied electrical field. This is schematically shown in the inset of Fig. 17. The wide spectra may come from the following reasons. First, the transition comes from the bound subband to the continuum, which typically yields a large width of the absorption peak [68]. Second, the dot size and the Ge content variations may also play an important role. The Ge dot uniformity at this growth temperature is not very high [29]. Third, the use of high doping level may be another factor. Holes can be excited from many sublevels to the valence band edge, thus broadening the absorption spectrum. Next the intensity increases with increasing temperature. This is reasonable since at lower temperatures, holes are frozen and the absorption is reduced. The dips in the spectra are most likely due to the interference of the epi-layer as well as the absorption in the atmosphere.

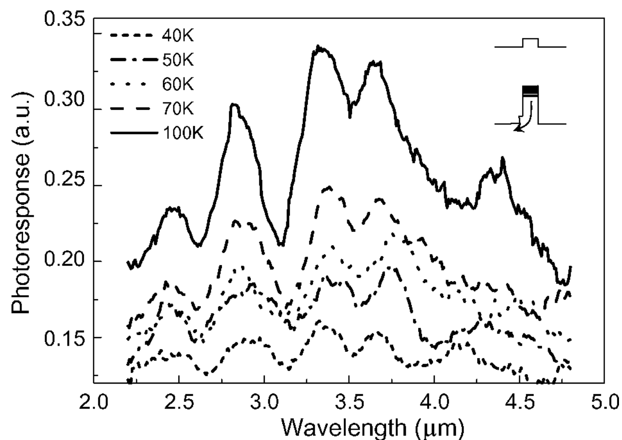


**Fig. 17.** ***Photoresponse spectra at different measurement temperatures. The growth temperature for the sample was 700 °C, and the doping level was 6 × 10$^{18}$ cm$^{-3}$ [67].***

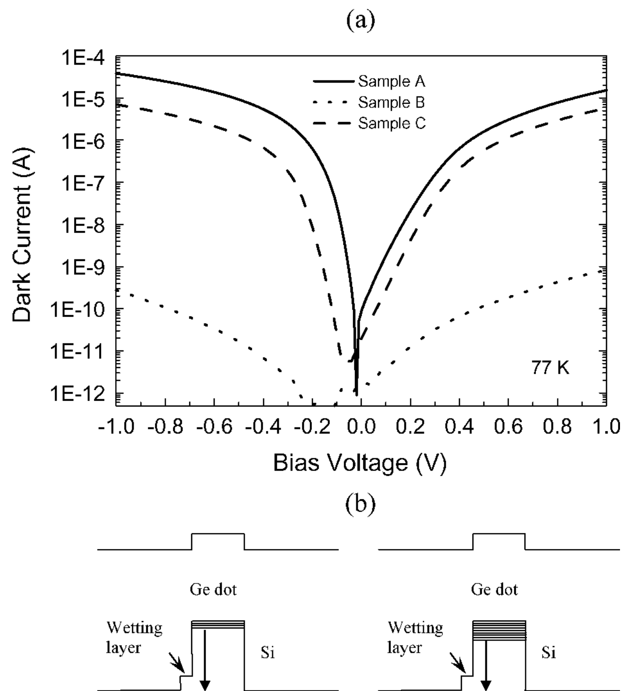


**Fig. 16.** ***(a) Dark current-voltage curves measured at 77 K for samples A, B, and C with different doping densities in the Ge dots and different spacer layer thicknesses. The device size was 500 × 500 $\mu$m$^2$. (b) Band diagrams showing that a higher doping level (right) tends to have holes filling the dot to higher hole energy sublevels comparing to the low doping level case (left) [67]. A higher dark current is resulted from the higher doping density as shown in (a).***

## VII. MID-INFRARED AND FAR-INFRARED Ge QUANTUM DOT n-i-n PHOTODETECTORS

For high responsivity applications, photodetectors with n-type active regions are favorable since p-type devices usually have very low carrier lifetime due to the large effective mass and the complicated valence band structure in Si and Ge [69], [70]. But there is a major obstacle for n-type SiGe based materials; a much smaller band offset in the conduction band as compared to the valence band [71], [72]. For low Ge contents, there is the vanishing normal incidence absorption for intersubband transitions due to the Si-like band structure. For high Ge contents, n-type detectors with normal incidence detection may be possible due to the nonvanishing off-diagonal mass tensor in (100) Ge dots grown on Si substrate. In this case, the sublevels in the active region of the photodetector are formed by using a phosphorus $\delta$-doping, for example, [73], [74]. Also the carrier lifetime can be increased due to the quantum confinement effect in the dots.

A 500 nm n$^+$ doped Si buffer layer was first grown at 600 °C on n-type Si (100) substrates by solid-source MBE. A set of a doped Ge dot layer and a 200 nm intrinsic Si

spacer was repeated two times at 540 °C. Then Ge dot layer with a nominal coverage of 1.5 nm and a phosphorus doping of $5 \times 10^{19}$ cm$^{-3}$ was grown. The structure was completed with a 50 nm heavily doped Si on top as the contact layer. The samples were processed into $500 \times 500$ $\mu$m$^2$ mesa diodes and Ti/Al films were deposited to form the contacts. The $I$–$V$ characteristics were measured with HP4145B. The photoresponse was characterized at normal incidence using a glow bar coupled with a monochromator whose light was chopped at 2 kHz.

Dark current-voltage characteristics at four different temperatures are shown in Fig. 18. A strong temperature dependence is evident as the direct result of the thermal activation of electrons in the active region. At 15 K, the current is 6.7 nA at +3 V. The relatively flat region below +1.7 V at 15 K is due to the photocurrent from the room temperature background radiation. The device has a breakdown voltage of ~7 V in the forward bias.

The response spectrum in the mid-IR region is shown in Fig. 19(a). The spectrum shows that the device has a response covering the whole mid-IR range. The dips in the spectra are considered to be from the atmospheric absorption and/or the interference effect of the epi-layer. Fig. 19(b) shows the response spectra in the far-IR range. To clarify the signal in the 16–20 $\mu$m region, which could possibly be originated from the 2nd order diffraction of 8–10 $\mu$m light, an mercury cadmium telluride (MCT) detector with a cutoff wavelength at 12 $\mu$m was used to check the system. By the different features presented in the spectra for MCT and our devices, it was concluded that our device had a response in the 16–20 $\mu$m range. Thus, the device has a response covering all the mid-IR through far-IR ranges. Fig. 19(b) also indicates that the response intensity is significantly enhanced with the increase of the bias. The results show a ~50 times signal enhancement for 6 V compared to 1.5 V bias. The undulation in the spectra may also be due to the atmospheric absorption.

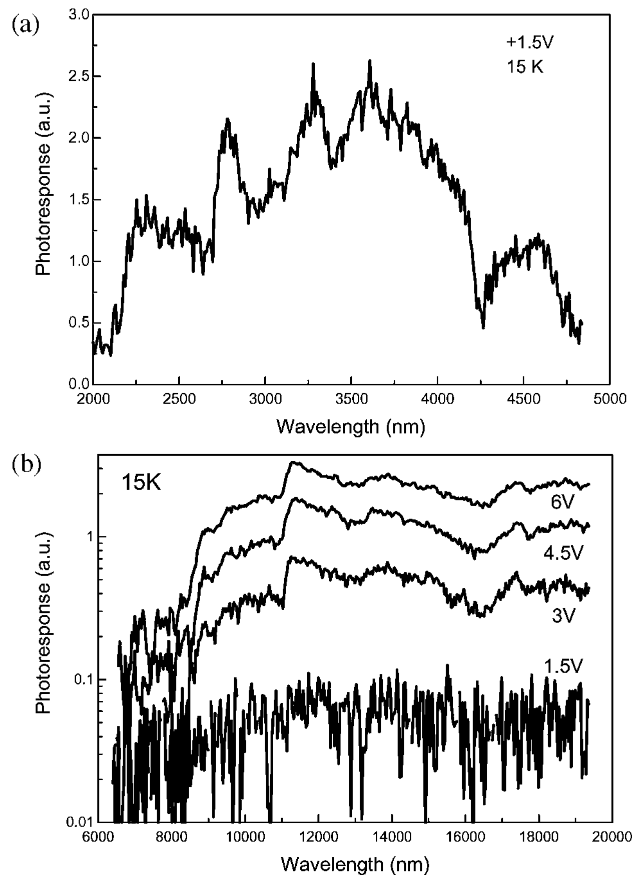


**Fig. 19.** ***(a) Photoresponse spectrum in the mid-IR range at 1.5 V bias taken with a 2–5 $\mu$m bandpass filter. (b) Spectra in the far-IR range at various biases taken with an 8–25 $\mu$m bandpass filter. Note that in this plot, the y axis is in a logarithmic scale. Normal incidence was used for both (a) and (b).***

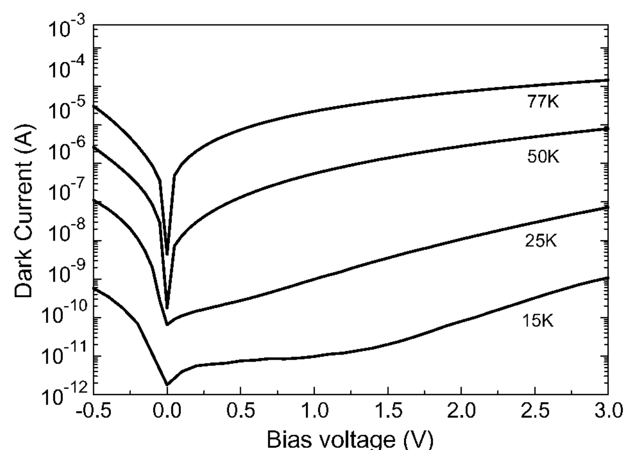


**Fig. 18.** ***Dark current-voltage curves at 15, 25, 50, and 77 K for the 500 × 500 $\mu$m$^2$ device.***

The photoresponse is ascribed to the transitions of electrons in the Ge dots. Without doping, it is well established that the Ge dot on Si has a type-II band alignment with the main offset in the valence band, as shown above. However, with phosphorus-doping in the Ge regions, self-consistent potential wells are induced in the conduction band in this case. Quantized energy levels are formed due to the reduced dimensionality of a few nanometers height Ge dots in the growth direction. Electrons occupy the low-energy levels. Excitation of electrons from the ground state to higher-energy levels and the conduction-band edge by absorbing photons generates photocurrent under the applied electric field. The broad response spectra may come from different sizes of the dots, as well as from the fact that more than one quantum levels are involved in the absorption.

Since the energy minima in the conduction band for Ge lie in the L ellipsoids along ⟨111⟩ directions, the inverse electron mass tensor for Ge (100) has nonvanishing off-diagonal elements [75]. Thus, there is a normal incidence absorption induced via intersubband transitions of electrons for the Ge wells grown on Si (100) substrate.

## VIII. NEAR-INFRARED p-i-n Ge QUANTUM DOT PHOTODETECTORS OPERATING AT 1.31–1.55 $\mu$m

In this section, we describe the fabrication and properties of near-infrared p-i-n Ge quantum-dot photodetectors. This approach takes the advantage of the interband transition in the type-II aligned band structure as well as full compatibility with modern Si technology. By properly tailoring growth parameters, it is possible to apply Ge quantum dots for 1.3–1.55 $\mu$m optical communication applications.

Using a normal-incidence configuration, the photocurrent (PC) of a p-i-n photodetector was measured at both 77 K and room temperature. A tungsten lamp was used as a light source. The light passed through a 34 cm monochromator and cast normally onto the diode. An 850 nm low-pass filter was placed in front of the device.

Fig. 20 shows both PC data for the fabricated dot diode and a standard Si photodiode with no bias applied. The quantum-dot sample has two peaks. One is related to the Si absorption at the low wavelength, ranging from 850 to 1250 nm and the other at the higher wavelength is related to the Ge dots. The photoresponse range of the Si photodiode extends to 1. 15 $\mu$m, which corresponds to the Si bandgap. The main peak of the quantum-dot sample extends to 1.25 $\mu$m.

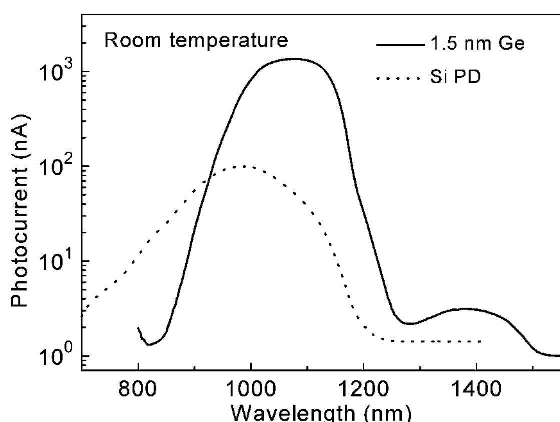


**Fig. 20.** ***A comparison of the photoresponse spectra between a quantum-dot diode and a Si photodiode at room temperature with no bias. The quantum-dot diode exhibits two peaks, which are related to Si absorption at a shorter wavelength range and Ge dots at a longer wavelength range, respectively.***

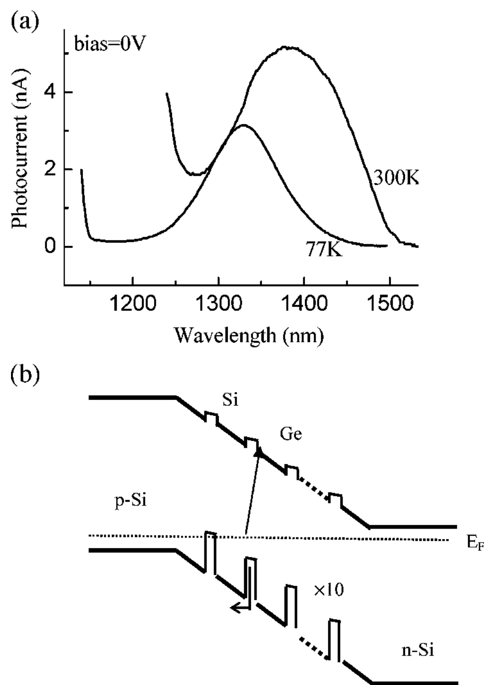


**Fig. 21.** ***(a) Two short circuit photocurrent curves of the Ge dot detector at room temperature and 77 K, respectively. At room temperature, the response covers the range from 1.3 to 1.52 $\mu$m with a peak response at 1.4 $\mu$m. The response peak shifts to 1.32 $\mu$m at 77 K. (b) Schematic band diagram of the dot structure at no bias.***

This may come from the absorption of the interdiffused wetting layers [76].

The PC spectra of the quantum-dot p-i-n photodiode measured at both room temperature and 77 K are shown in Fig. 21(a). As the temperature decreases from room temperature to 77 K, the peak shifts from 1.4 to 1.32 $\mu$m. The FWHM also shrinks from 95 to 70 meV and the photoresponse intensity shows a clear decrease. Fig. 21(b) illustrates a possible mechanism to explain the observed photoresponse of the diode. Previous works indicate that Ge dots embedded in Si have a type-II band alignment. For the PC process, the photocurrent only originates from the Ge/Si interface regions when the photon energy is low. The absorption occurs both in the regions near the interfaces and in the dots when the energy is high enough. The electron–hole pairs then contribute to conduction current via thermionic emission. It is clear that the photocurrent peak response comes from the electron–hole pairs generated in the energy range from the transition from the valence band ground state level of the Ge dot to the conduction band of Si, to the energy from the valence edge of Si to the conduction band of Ge. On the other hand, for PL, the excited holes nearby will drift to the Ge dots very rapidly, and electrons will drift away from dots. As a result, the recombination responsible for the observed PL peaks occurs at the Ge/Si interfaces.

Fig. 22 presents the dependence of the photoresponse spectrum on applied reverse bias at room temperature. As the bias increases, the photoresponse increases but the shape of the curve remains almost unchanged. There is no clear shift in the cutoff wavelength (less than 10 nm). Due to the low applied voltage on the devices, the quantum confined Stark effect is weak. The high measurement temperature may also obscure the quantum confined Stark effect. Similar results were also observed in SiGe quantum wells and superlattices [77]. The external efficiency at the peak wavelength of 1.4 $\mu$m is 8% at 2.5 V estimated from the excitation power of 360 nW. This efficiency is comparable to that of the Ge/Si strained layer superlattice (12%) grown by MBE operating at 1.3 $\mu$m under a waveguide coupling mode as reported by Splett *et al.* [78].

The PC spectra of three samples at room temperature are shown in Fig. 23. These samples contain nominal Ge thicknesses of 1.2, 1.5, and 1.8 nm in each period. All the samples show a photoresponse peak in the region of between 1.3 and 1.55 $\mu$m. It also shows that as the Ge nominal growth thickness increases, the photoresponse peak shifts slightly to longer wavelength. This is due to the fact that the Ge dot height increases with increasing nominal growth thickness, and this in turn reduces the ground state energy of holes in the dots. However, the shift is small. It is important to note that the dots are not pure Ge. From a separate grazing incidence X-ray diffraction measurement [79], the average Ge content of the dot is about 55%. A 0.88 eV fundamental gap can be extracted for this content according to Reiger and Vogl's theoretical work [71]. The result is in agreement with our PC result that shows the peak response of around 0.88 eV. The cutoff transition energy is, however, 0.83 eV, i.e., 50 meV lower. The possible reason for this difference is the presence of the conduction band offset, which has a negative contribution to the transition energy.

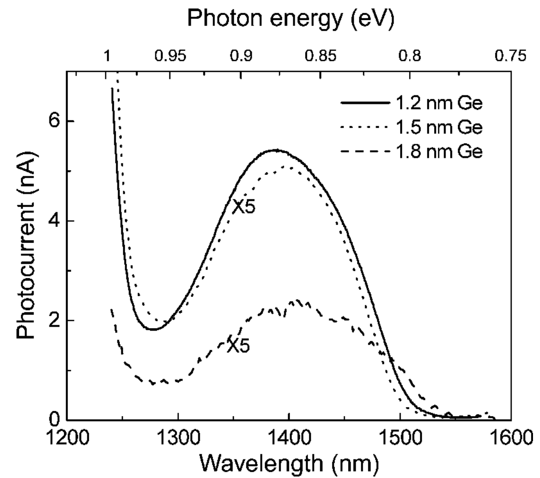


**Fig. 23.** ***Photoresponse spectra for three samples with different dot thicknesses at room temperature. As the nominal Ge thickness increases from 1.2 to 1.8 nm, the peak response shifts slightly to a longer wavelength, due to the lower transition energy of the shallower hole sublevel energy.***

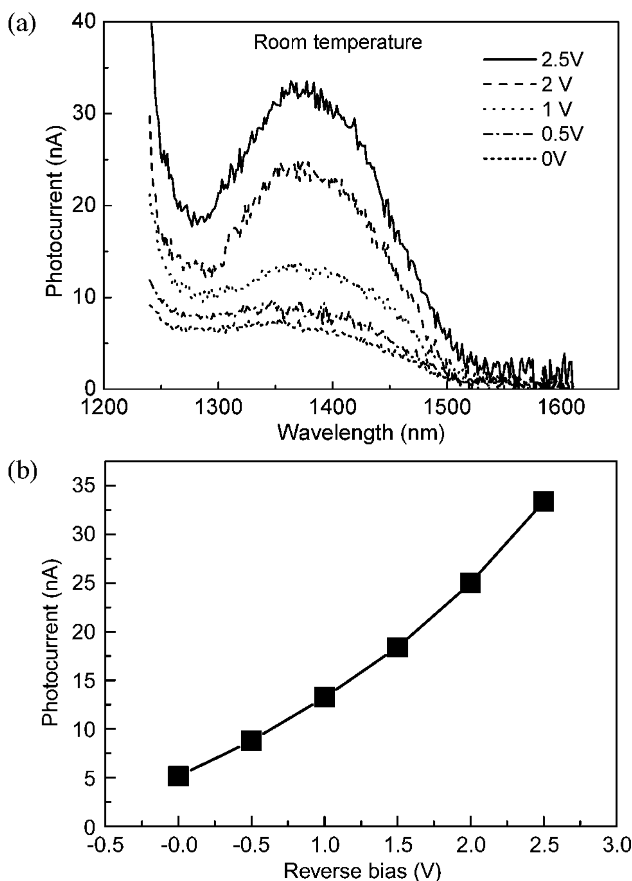


**Fig. 22.** ***(a) Photoresponse spectra at different applied reverse biases. (b) The photoresponse intensity as a function of reverse bias under an illumination power of 360 nW. The response wavelength is selected at 1.4 $\mu$m. The maximum external efficiency is estimated to be 8% at 2.5 V.***

## IX. Ge QUANTUM DOT LIGHT-EMITTING DIODES

The development of optical networks based on wavelength division multiplexing is stimulating the research for low-cost optical components. Low-cost components in the fiber optic communication wavelengths based on silicon are of great interest due to the possible integration with the well-developed Si-based technology. These components such as photodetectors and light-emitting sources are expected to operate in the near infrared spectral range around the 1.3–1.55 $\mu$m. Due to the indirect band nature of Si, a luminescence efficiency of Si-based structures is very low. Thus, there are tremendous efforts to make efficient light emitters on Si through the incorporating of Ge/Si self-assembled nanostructures in an active layer of a diode.

A p-i-n structure consists of 10-period intrinsic multilayered Ge quantum dots sandwiched with an n-type and a p-type Si layers on an n-doped Si (100) substrate. For this sample, the growth temperature was kept at 550 °C. After an 100 nm undoped Si buffer layer, a 300 nm $n^+$ Si layer was grown with an Sb doping concentration of $\sim 2 \times 10^{18}$ cm$^{-3}$, followed by a 50 nm intrinsic Si. Then ten multilayers were grown with an 8 ML Ge layer and an undoped Si barrier layer of 20 nm thick; after a 100 nm undoped Si space layer a 100 nm $p^+$ Si contact layer was then grown with a boron doping concentration of $5 \times 10^{18}$ cm$^{-3}$. Mesas were defined by optical lithography and dry etching with $CF_4/O_2$ or wet etching with tetramethylammonium hydroxide (TMAH). The mesa size is $150 \times 300$ $\mu m^2$. A 220 nm $SiO_2$ isolation layer was deposited by plasma enhanced chemical vapor deposition (PECVD) and an Al/Ti layer was deposited for contact.

The current–voltage characteristics of a typical diode at room temperature are shown in Fig. 24. A low leakage current of $3 \times 10^{-5}$ A/cm$^2$ at $-1$ V was obtained and the breakdown voltage was measured to be 7 V at room temperature. This is similar to the results of obtained by Splett, where Si/Ge strained layer superlattices were used instead [78]. Due to high generation rates in Ge, there was a high leakage current. The electroluminescence (EL) was excited with square electrical pulses at a low frequency with a 1 : 1 duty cycle. A liquid-nitrogen cooled Ge photodiode was used for EL spectra measurement. Fig. 25(a) shows EL spectra measured at 77 K as a function of the current density. The NP-Si peak occurs at around 1.1 $\mu$m, while the peak at about 1.33 $\mu$m is due to the EL from the quantum dots, which may consist of two peaks of NP and TO-assisted ones. The broad peak at around 1.48 $\mu$m may be due to a radiative intraband transition [80]. The EL results at room temperature are shown in Fig. 25(b). The EL peak of 1.33 $\mu$m from the quantum dots is clear. The results demonstrate the feasible application of Ge quantum dots for low-cost optical emitters operated at the telecommunication wavelengths and integrated on Si. However, the quantum efficiency will be still low and hence for practical applications, research in search for new highly efficient emission mechanisms remains the most important challenge.

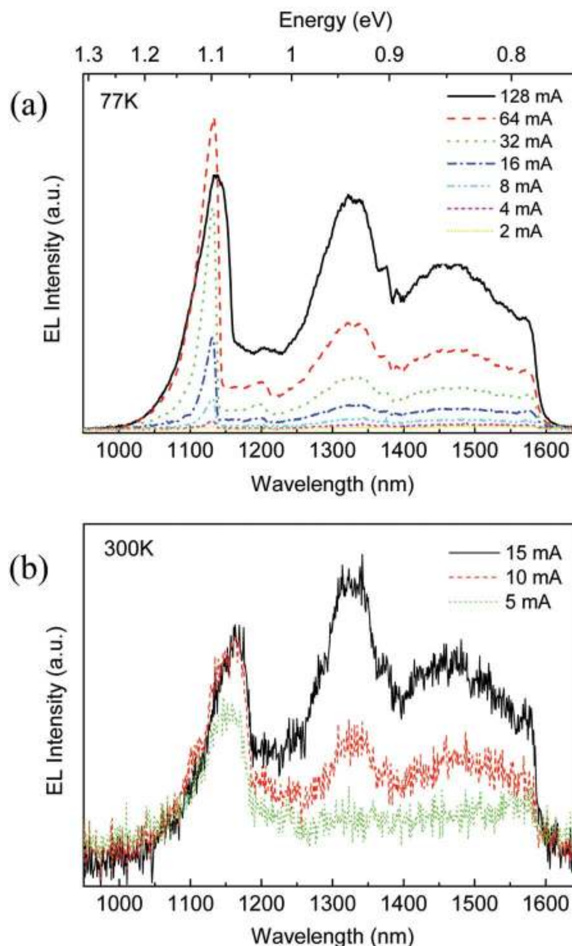


**Fig. 25.** ***Electroluminescence spectra at different biases measured at: (a) 77 K and (b) 300 K. Electroluminescence from quantum dots was observed at around 1.33 $\mu$m.***

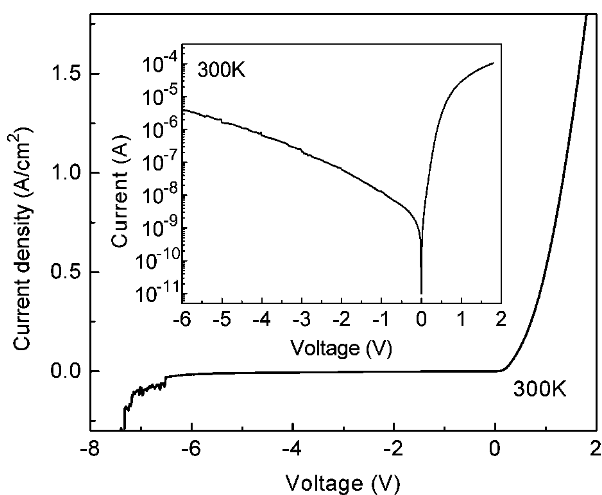


**Fig. 24.** ***Current–voltage characteristics of a Ge dot p-i-n diode at room temperature. The breakdown voltage is 7 V. The inset gives a semilog plot of the I–V characteristic, showing clearly a dark current density of $3 \times 10^{-5}$ A/cm$^2$ at $-1$ V.***

## X. SUMMARY

In summary, we have discussed the major issues involved in the growth, processing, and characterization of Ge dots, interband and intersubband properties of Ge dots, and their related optoelectronic devices on Si substrates. Self-assembled and guided Ge quantum dots, and Ge quantum-dot superlattices grown on Si (100) substrates were discussed. The morphology of dots was shown to

relate to growth rate, growth temperature, deposited coverage, postgrowth holding time, and doping. Uniformity and alignment controls of ultrasmall Ge dots and arrays are two key challenges for self-assembly grown Ge dots. Self-assembled Ge quantum dots with a lateral size as small as 30 nm, a height of ~5 nm, and a density as high as $10^{11}$ $cm^{-2}$ selectively grown in nanopatterns on a Si (001) substrate was demonstrated. This approach of using a self-assembled diblock copolymer to achieve nanopatterns on Si substrates for ordered Ge quantum dot holds a high promise. The vertical correlation was observed and analyzed in multilayered Ge quantum-dot layers. It was shown that the vertical correlation was maintained until the effective critical thickness of the superlattice was reached at which point, the threading dislocations developed. The dots then tended to nucleate around the edge of the pits induced by the threading dislocations. PL and FTIR were used to study the interband and intersubband transitions in the Ge dots. The PL on thicker superlattice showed dislocation-related peaks. Mid-infrared absorption was observed in $Si_{1-X}Ge_X$ quantum dots on prepatterned Si substrates prepared by a diblock copolymer process. The polarization dependence results show significant normal incidence absorption. Si-based IR photodetector with embedded Ge quantum dots was successfully developed. The devices grown at 700 °C had a normal-incident response range from 2.8 $\mu$m to 4.8 $\mu$m peaked at 3.5 $\mu$m. The response was due to the intersubband transitions of the holes in the self-assembled Ge dots. Normal incidence photodetectors were demonstrated using n-type Ge dot arrays grown on Si (100) substrate. The devices with n-i-n structures had a dark current density of 3 nA/$cm^2$ at +3 V with the response spectra covering the mid-infrared and far-infrared ranges. Pin intersubband photo-detectors using Ge dots were also discussed for the 1.3–1.5 $\mu$m communication applications and the response to this wavelength range was demonstrated. We have also demonstrated Ge quantum-dot light-emitting diodes. The wavelength of emitting light was in the region of 1.3–1.55 $\mu$m. ■

## Acknowledgment

The authors would like to thank the many collaborators. Among them are Masaaki Ogawa, Fei Liu, and Joo-Young Lee.

## REFERENCES


[1] T. P. Pearsall and J. C. Bean, "Enhancement- and depletion-mode p-channel $Ge_x$ $Si_{1-x}$ modulation-doped FET's," *IEEE Electron Device Lett.*, vol. EDL-7, no. 5, pp. 308–310, May 1986.

[2] H. Daembkes, H.-J. Herzog, H. Jorke, H. Kibbel, and E. Kasper, "The n-channel SiGe/Si modulation-doped field-effect transistor," *IEEE Trans. Electron Devices*, vol. ED-33, no. 5, pp. 633–638, May 1986.

[3] T. Tatsumi, H. Hirayama, and N. Aizaki, "Si/$Ge_{0.3}Si_{0.7}$/Si heterojunction bipolar transistor made with Si molecular beam epitaxy," *Appl. Phys. Lett.*, vol. 52, no. 11, pp. 895–897, Mar. 1988.

[4] D. K. Nayak, J. C. Woo, J. S. Park, K. L. Wang, and K. P. MacWilliams, "Enhancement-mode quantum-well $Ge_x$ $Si_{1-x}$ PMOS," *IEEE Electron Device Lett.*, vol. 12, no. 4, pp. 154–156, Apr. 1991.

[5] S. David, M. E. Kurdi, P. Boucaud, C. Kammerer, L. Xiang, S. Sauvage, V. Le Thanh, I. Sagnes, D. Bouchier, and J.-M. Lourtioz, "Ge/Si self-assembled islands integrated in 2D photonic crystal microcavities for realisation of silicon-based light-emitting devices," *Proc. SPIE*, vol. 5450, pp. 369–375, 2004.

[6] G. Masini, V. Cencelli, L. Colace, F. de Notaristefani, and G. Assanto, "Linear array of Si-Ge heterojunction photodetectors monolithically integrated with silicon CMOS readout electronics," *IEEE J. Sel. Topics Quantum Electron.*, vol. 10, no. 4, pp. 811–815, Jul.–Aug. 2004.

[7] L. Colace, G. Masini, V. O. Cencelli, F. de Notaristefani, and G. Assanto, "Polycrystalline germanium enables near-IR photodetectors integrated with silicon CMOS electronics," *Photon. Spectra*, vol. 38, no. 12, pp. 88–92, Dec. 2004.

[8] R. A. Soref, "Silicon-based optoelectronics," *Proc. IEEE*, vol. 81, no. 12, pp. 1687–1706, Dec. 1993.

[9] M. Herbst, C. Schramm, K. Brunner, T. Asperger, H. Riedl, G. Abstreiter, A. Vörckel, H. Kurz, and E. Müller, "Structural and optical properties of vertically correlated Ge island layers grown at low temperatures," *Mater. Sci. Eng. B*, vol. 89, no. 1–3, pp. 54–57, Feb. 2002.

[10] M. Elkurdi, P. Boucaud, S. Sauvage, O. Kermarrec, Y. Campidelli, D. Bensahel, G. Saint-Girons, and I. Sagnes, "Near-infrared waveguide photodetector with Ge/Si self-assembled quantum dots," *Appl. Phys. Lett.*, vol. 80, no. 3, pp. 509–511, Jan. 2002.

[11] R. Vrijen *et al.*, "Electron-spin-resonance transistors for quantum computing in silicon-germanium heterostructures," *Phys. Rev. A*, vol. 62, pp. 012306-1–012306-10, Jul. 2000.

[12] T. Kitajima, B. Liu, and S. R. Leone, "Two-dimensional periodic alignment of self-assembled Ge islands on patterned Si(001) surfaces," *Appl. Phys. Lett.*, vol. 80, no. 3, pp. 497–499, Jan. 2002.

[13] T. I. Kamins and R. S. Williams, "Lithographic positioning of self-assembled Ge islands on Si(001)," *Appl. Phys. Lett.*, vol. 71, no. 9, pp. 1201–1203, Sep. 1997.

[14] E. Kuramochi, J. Temmyo, H. Kamada, and T. Tamamura, "Spatial ordering of self-organized InGaAs/AlGaAs quantum disks on GaAs (311)B substrates," *J. Electron. Mater.*, vol. 28, no. 5, pp. 445–451, May 1999.

[15] A. Karmous, A. Cuenat, A. Ronda, I. Berbezier, S. Atha, and R. Hull, "Ge dot organization on Si substrates patterned by focused ion beam," *Appl. Phys. Lett.*, vol. 85, no. 26, pp. 6401–6403, Dec. 2004.

[16] E. Kim, N. Usami, and Y. Shiraki, "Control of Ge dots in dimension and position by selective epitaxial growth and their optical properties," *Appl. Phys. Lett.*, vol. 72, no. 13, pp. 1617–1619, Mar. 1998.

[17] A. I. Yakimov, A. V. Dvurechenskii, A. I. Nikiforov, A. A. Bloshkin, A. V. Nenashev, and V. A. Volodin, "Electronic states in Ge/Si quantum dots with type-II band alignment initiated by space-charge spectroscopy," *Phys. Rev. B*, vol. 73, pp. 115333-1–115333-8, Mar. 2006.

[18] T. Takagahara and K. Takeda, "Theory of the quantum confinement effect on excitons in quantum dots of indirect-gap materials," *Phys. Rev. B*, vol. 46, pp. 15578–15581, Dec. 1992.

[19] S. Y. Ren, "Quantum confinement of edge states in Si crystallites," *Phys. Rev. B*, vol. 55, pp. 4665–4669, Feb. 1997.

[20] O. G. Schmidt, C. Lang, and K. Eberl, "Photoluminescence study of the 2D-3D growth mode changeover for different Ge/Si island phases," *Phys. Stat. Sol. B*, vol. 215, pp. 319–324, Sep. 1999.

[21] C. S. Peng, Q. Huang, W. Q. Cheng, J. M. Zhou, Y. H. Zhang, T. T. Sheng, and C. H. Tung, "Optical properties of Ge self-organized quantum dots in Si," *Phys. Rev. B*, vol. 57, pp. 8805–8808, Apr. 1998.

[22] D. N. Lobanov, A. V. Novikov, N. V. Vostokov, Y. N. Drozdov, A. N. Yablonskiy, Z. F. Krasilnik, M. Stoffel, U. Denker, and O. G. Schmidt, "Growth and photoluminescence of self-assembled islands obtained during the deposition of Ge on a strained SiGe layer," *Opt. Mater.*, vol. 27, no. 5, pp. 818–821, Feb. 2005.

[23] N. V. Vostokov, Z. F. Krasil'nik, D. N. Lobanov, A. V. Novikov, M. V. Shaleev, and A. N. Yablonsky, "Influence of the germanium deposition rate on the growth and photoluminescence of Ge(Si)/Si(001) self-assembled islands," *Phys. Solid State*, vol. 47, no. 1, pp. 38–41, 2005.

[24] M. Larsson, A. Elfving, P. O. Holtz, G. V. Hansson, and W.-X. Ni, "Photoluminescence study of Si/Ge quantum dots," *Surf. Sci.*, vol. 532–535, pp. 832–836, Jun. 2003.

[25] L. Martinelli, A. Marzegalli, P. Raiteri, M. Bollani, F. Montalenti, L. Miglio, D. Chrastina, G. Isella, and H. Kanel, "Formation of strain-induced Si-rich and Ge-rich nanowires at misfit dislocations in SiGe: A model supported by photoluminescence data," *Appl. Phys. Lett.*, vol. 84, no. 15, pp. 2895–2897, Apr. 2004.

[26] L. Vescan, T. Stoica, O. Chretien, M. Goryll, E. Mateeva, and A. Muck, "Size distribution and electroluminescence of self-assembled Ge dots," *J. Appl. Phys.*, vol. 87, no. 10, pp. 7275–7282, May 2000.

[27] K. N. Tu, J. W. Mayer, and L. C. Feldman, *Electronic Thin Film Science: For Electrical Engineers and Materials Scientists*. New York: Macmillan, 1992, ch. 7, pp. 167–168.

[28] D. J. Eaglesham and M. Cerullo, "Dislocation-free Stranski-Krastanow growth of Ge on Si(100)," *Phys. Rev. Lett.*, vol. 64, pp. 1943–1946, Apr. 1990.

[29] G. Jin, J. L. Liu, and K. L. Wang, "Temperature effect on the formation of uniform self-assembled Ge dots," *Appl. Phys. Lett.*, vol. 83, no. 14, pp. 2847–2849, Oct. 2003.

[30] G. Medeiros-Ribeiro, A. M. Bratkovski, T. I. Kamins, D. A. A. Ohlberg, and R. S. Williams, "Shape transition of germanium nanocrystals on a silicon (001) surface from pyramids to domes," *Science*, vol. 279, pp. 353–355, Jan. 1998.

[31] R. M. Ross, R. M. Tromp, and M. C. Reuter, "Transition states between pyramids and domes during Ge/Si island growth," *Science*, vol. 286, pp. 1931–1934, Dec. 1999.

[32] V. A. Shchukin, N. N. Ledentsov, P. S. Kopev, and D. Bimberg, "Spontaneous ordering of arrays of coherent strained islands," *Phys. Rev. Lett.*, vol. 75, pp. 2968–2971, Oct. 1995.

[33] T. I. Kamins, E. C. Carr, R. S. Williams, and S. J. Rosner, "Deposition of three-dimensional Ge islands on Si(001) by chemical vapor deposition at atmospheric and reduced pressures," *J. Appl. Phys.*, vol. 81, no. 1, pp. 211–219, Jan. 1997.

[34] K. L. Wang, J. L. Liu, and G. Jin, "Self-assembled Ge quantum dots on Si and their applications," *J. Cryst. Growth*, vol. 237–239, pp. 1892–1897, Apr. 2002.

[35] J. Drucker and S. Chaparro, "Diffusional narrowing of Ge on Si(100) coherent island quantum dot size distributions," *Appl. Phys. Lett.*, vol. 71, no. 5, pp. 614–616, Aug. 1997.

[36] T. I. Kamins, G. Medeiros-Ribeiro, D. Ohlberg, and R. S. Williams, "Evolution of Ge islands on Si(001) during annealing," *J. Appl. Phys.*, vol. 85, no. 2, pp. 1159–1171, Jan. 1999.

[37] J. A. Floro, G. A. Lucadamo, E. Chason, L. B. Freund, M. Sinclair, R. D. Twesten, and R. Q. Hwang, "SiGe island shape transitions induced by elastic repulsion," *Phys. Rev. Lett.*, vol. 80, pp. 4717–4720, May 1998.

[38] F. Boscherini, G. Capellini, L. di Gaspare, F. Rosein, N. Motta, and S. Mobilio, "Ge–Si intermixing in Ge quantum dots on Si(001) and Si(111)," *Appl. Phys. Lett.*, vol. 76, no. 6, pp. 682–684, Feb. 2000.

[39] X. Z. Liao, J. Zou, D. Cockayne, J. Qin, Z. M. Jiang, X. Wang, and R. Leon, "Strain relaxation by alloying effects in Ge islands grown on Si(001)," *Phys. Rev. B*, vol. 60, pp. 15 605–15 608, Dec. 1999.

[40] K. Sakamoto, H. Matsuhata, M. O. Tanner, D. Wang, and K. L. Wang, "Alignment of Ge three-dimensional islands on faceted Si(001) surfaces," *Thin Solid Films*, vol. 321, pp. 55–59, May 1998.

[41] Y. H. Xie, S. B. Samavedam, M. Bulsara, T. A. Langdo, and E. A. Fitzgerald, "Relaxed template for fabricating regularly distributed quantum dot arrays," *Appl. Phys. Lett.*, vol. 71, no. 24, pp. 3567–3568, Dec. 1997.

[42] S. Y. Shirgaev, E. V. Pedersen, F. Jensen, J. W. Petersen, J. L. Hansen, and A. N. Larsen, "Dislocation patterning—A new tool for spatial manipulation of Ge islands," *Thin Solid Films*, vol. 294, pp. 311–314, Feb. 1997.

[43] Q. Xie, A. Madhukar, P. Chen, and N. P. Kobayashi, "Vertically self-organized InAs quantum box islands on GaAs(100)," *Phys. Rev. Lett.*, vol. 75, pp. 2542–2545, Sep. 1995.

[44] C. Teichert, J. Tersoff, and M. G. Lagally, "Stress-induced self-organization of nanoscale structures in SiGe/Si multilayer films," *Phys. Rev. B*, vol. 53, pp. 16 334–16 337, Jun. 1996.

[45] G. Jin, J. L. Liu, S. G. Thomas, Y. H. Luo, K. L. Wang, and B. Y. Nguyen, "Controlled arrangement of self-organized Ge islands on patterned Si (001) substrates," *Appl. Phys. Lett.*, vol. 75, no. 18, pp. 2752–2754, Nov. 1999.

[46] G. Jin, J. L. Liu, and K. L. Wang, "Regimented placement of self-assembled Ge dots on selectively grown Si mesas," *Appl. Phys. Lett.*, vol. 76, no. 24, pp. 3591–3593, Jun. 2000.

[47] R. R. Li, P. D. Dapkus, M. E. Thompson, W. G. Jeong, C. Harrison, P. M. Chaikin, R. A. Register, and D. H. Adamson, "Dense arrays of ordered GaAs nanostructures by selective area growth on substrates patterned by block copolymer lithography," *Appl. Phys. Lett.*, vol. 76, no. 13, pp. 1689–1691, Mar. 2000.

[48] Z. M. Zhao, T. S. Yoon, W. Feng, B. Y. Li, J. H. Kim, J. Liu, O. Hulko, Y. H. Xie, H. M. Kim, K. B. Kim, K. L. Wang, C. Ratsch, R. Caflisch, D. Y. Ryu, and T. P. Russell, "The challenges in guided self-assembly of Ge and InAs quantum dots on Si," *Thin Solid Films*, vol. 508, pp. 195–199, Jun. 2006.

[49] D. Cha, M. Ogawa, C. Chen, S. Kim, J. Lee, K. L. Wang, J. Wang, and T. P. Russell, "Intersubband absorption in p-type $Si_{1-x}Ge_x$ quantum dots on pre-patterned Si substrates made by a diblock copolymer process," *J. Cryst. Growth*, vol. 301–302, pp. 833–836, Apr. 2007.

[50] D. Y. Ryu, K. Shin, E. Drokenmuller, C. J. Hawker, and T. P. Russell, "A generalized appproach to the modification of solid surfaces," *Science*, vol. 308, pp. 236–239, Apr. 2005.

[51] P. Mansky, Y. Liu, E. Huang, T. P. Russell, and C. Hawker, "Controlling polymer-surface interactions with random copolymer brushes," *Science*, vol. 275, pp. 1458–1460, Mar. 1997.

[52] O. G. Schmidt, O. Kienzle, Y. Hao, K. Eberl, and F. Ernst, "Modified Stranski–Krastanov growth in stacked layers of self-assembled islands," *Appl. Phys. Lett.*, vol. 74, no. 9, pp. 1272–1274, Mar. 1999.

[53] C. Teichert, M. G. Lagally, L. J. Peticolas, J. C. Bean, and J. Tersoff, "Stress-induced self-organization of nanoscale structures in SiGe/Si multilayer films," *Phys. Rev. B*, vol. 53, pp. 16 334–16 337, Jun. 1996.

[54] J. Tersoff, C. Teichert, and M. G. Lagally, "Self-organization in growth of quantum dot superlattices," *Phys. Rev. Lett.*, vol. 76, pp. 1675–1678, Mar. 1996.

[55] B. Rahmati, W. Jaeger, H. Trinkaus, R. Loo, L. Vescan, and H. Lueth, "Vertical ordering of islands in Ge-Si multilayers," *Appl. Phys. A*, vol. 62, pp. 575–579, 1996.

[56] O. Kienzle, F. Ernst, M. Ruhle, O. G. Schmidt, and K. Eberl, "Germanium 'quantum dots' embedded in silicon: Quantitative study of self-alignment and coarsening," *Appl. Phys. Lett.*, vol. 74, no. 2, pp. 269–271, Jan. 1999.

[57] R. People and J. C. Bean, "Calculation of critical layer thickness versus lattice mismatch for $Ge_xSi_{1-x}$/Si strained-layer heterostructures," *Appl. Phys. Lett.*, vol. 47, no. 3, pp. 322–324, Aug. 1985.

[58] C. G. van de Walle and R. M. Martin, "Theoretical study of Si/Ge interfaces," *J. Vac. Sci. Technol. B*, vol. 3, pp. 1256–1259, Jul./Aug. 1985.

[59] F. Liu, S. Tong, J. Liu, and K. L. Wang, "Normal incident mid-infrared Ge quantum dot photodetector," *J. Electron. Mater.*, vol. 33, no. 8, pp. 846–850, 2004.

[60] Y. Y. Lin and J. Singh, "Theory of polarization dependent intersubband transitions in *p*-type SiGe/Si self-assembled quantum dots," *J. Appl. Phys.*, vol. 96, no. 2, pp. 1059–1063, Jul. 2004.

[61] U. Bockelmann and G. Bastard, "Phonon scattering and energy relaxation in two-, one-, and zero-dimensional electron gases," *Phys. Rev. B*, vol. 42, pp. 8947–8951, Nov. 1990.

[62] J. Phillips, K. Kamath, and P. Bhattacharya, "Far-infrared photoconductivity in self-organized InAs quantum dots," *Appl. Phys. Lett.*, vol. 72, no. 16, pp. 2020–2022, Apr. 1998.

[63] N. Rappaport, E. Finkman, T. Brunhes, P. Boucaud, S. Sauvage, N. Yam, V. Le Thanh, and D. Bouchier, "Midinfrared photoconductivity of Ge/Si self-assembled quantum dots," *Appl. Phys. Lett.*, vol. 77, no. 20, pp. 3224–3226, Nov. 2000.

[64] T. Fromherz, W. Mac, A. Hesse, G. Bauer, C. Miesner, K. Brunner, and G. Abstreiten, "Intraband absorption and photocurrent spectroscopy of self-assembled *p*-type Si/SiGe quantum dots," *Appl. Phys. Lett.*, vol. 80, no. 12, pp. 2093–2095, Mar. 2002.

[65] C. Miesner, O. Rothig, K. Brunner, and G. Abstreiter, "Intra-valence band photocurrent spectroscopy of self-assembled Ge dots in Si," *Appl. Phys. Lett.*, vol. 76, no. 8, pp. 1027–1029, Feb. 2000.

[66] M. S. Hegazy, T. F. Refaat, M. N. Abedin, and H. E. Elsayed-Ali, "Fabrication of Ge/Si quantum-dot infrared photodetector by pulsed laser deposition," *Optical Engineering*, vol. 44, no. 5, pp. 59702-1–59702-3, May 2005.

[67] S. Tong, J.-Y. Lee, H.-J. Kim, F. Liu, and K. L. Wang, "Ge dot mid-infrared photodetectors," *Opt. Mater.*, vol. 27, no. 5, pp. 1097–1100, Feb. 2005.

[68] B. F. Levine, "Quantum-well infrared photodetectors," *J. Appl. Phys.*, vol. 74, no. 8, pp. R1–R81, Oct. 15, 1993.

[69] W. Heiss, E. Gornik, H. Hertle, B. Murdin, G. M. H. Knippels, C. J. G. M. Langerak, F. Schaffler, and C. R. Pidgeon, "Determination of the intersubband lifetime in Si/SiGe quantum wells," *Appl. Phys. Lett.*, vol. 66, no. 24, pp. 3313–3315, Jun. 1995.

[70] I. Bormann, K. Brunner, S. Hackenbuchner, G. Abstreiter, S. Schmult, and W. Wegscheider, "Nonradiative relaxation times in diagonal transition Si/SiGe quantum cascade structures," *Appl. Phys. Lett.*, vol. 83, no. 26, pp. 5371–5373, Dec. 2003.

[71] M. M. Rieger and P. Vogl, "Electronic-band parameters in strained $Si_{1-x}Ge_x$ alloys on $Si_{1-y}Ge_y$ substrates," *Phys. Rev. B*, vol. 48, pp. 14 276–14 287, Nov. 1993.

[72] C. Chen, D. Cha, J. Lee, H. Kim, F. Liu, S. Tong, K. L. Wang, J.-Y. Wang, and

T. P. Russell, "Nano-patterned growth of Ge quantum dots for infrared detector applications," *Proc. Mater. Res. Soc. Symp.*, vol. 891, pp. 0891-EE06-01.1–0891-EE06-01.6, 2006.

[73] D. D. Coon and R. P. G. Karunasiri, "New mode of IR detection using quantum wells," *Appl. Phys. Lett.*, vol. 45, no. 6, pp. 649–651, Sep. 1984.

[74] L. C. West and S. J. Eglash, "First observation of an extremely large-dipole infrared transition within the conduction band of a GaAs quantum well," *Appl. Phys. Lett.*, vol. 46, no. 12, pp. 1156–1158, Jun. 1985.

[75] K. L. Wang and R. P. G. Karunasiri, "Infrared detectors using SiGe/Si quantum well structures," in *Semiconductor Quantum Wells and Superlattices for Long-Wavelength Infrared Detectors*, M. O. Manasreh, Ed. Norwood, MA: Artech House, 1993.

[76] J. Wan, G. L. Jin, Z. M. Jiang, Y. H. Luo, J. L. Liu, and K. L. Wang, "Band alignments and photon-induced carrier transfer from wetting layers to Ge islands grown on Si(001)," *Appl. Phys. Lett.*, vol. 78, no. 12, pp. 1763–1765, Mar. 2001.

[77] J. Y. Kim, S. Fukatsu, N. Usami, and Y. Shiraki, "Field-driven blue shift of excitonic photoluminescence in Si-Ge quantum wells and superlattices," *J. Cryst. Growth*, vol. 157, pp. 40–44, Dec. 1995.

[78] A. Splett, T. Zinke, K. Petermann, E. Kasper, H. Kibbel, H.-J. Herzog, and H. Presting, "Integration of waveguides and photodetectors in SiGe for 1.3 $\mu$m operation," *IEEE Photon. Technol. Lett.*, vol. 6, no. 1, pp. 59–61, Jan. 1994.

[79] Z. M. Jiang, X. M. Jiang, W. R. Jiang, Q. J. Jia, W. L. Zheng, and D. C. Qian, "Lattice strains and composition of self-organized Ge dots grown on Si(001)," *Appl. Phys. Lett.*, vol. 76, no. 23, pp. 3397–3399, Jun. 2000.

[80] W. Haecker, "Infrared radiation from breakdown plasmas in Si, GaSb, and Ge: Evidence for direct free hole radiation," *Phys. Stat. Sol. (a)*, vol. 25, pp. 301–310, Sep. 1974.

## ABOUT THE AUTHORS

**Kang L. Wang** (Fellow, IEEE) received the B.S. degree from National Cheng Kung University, China, in 1964, and the M.S. and Ph.D. degrees from the Massachusetts Institute of Technology (MIT), Cambridge, in 1966 and 1970, respectively.

From 1970 to 1972, he was an Assistant Professor at MIT. From 1972 to 1979, he worked at the General Electric Corporate Research and Development Center as a Physicist/Engineer. In 1979, he joined the Electrical Engineering Department, University of California, Los Angeles (UCLA), where he is currently Raytheon Chair Professor of Physical Electronics. He also served as Chair of the Department of Electrical Engineering at UCLA from 1993 to 1996. He also serves as the Director of the FCRP Focus Center on Functional Engineered Nano Architectonics—FENA, an interdisciplinary research center. He was also named the Director of the Western Institute of Nanoelectronics (WIN), a coordinated multiproject research institute with UCLA, Stanford University, UC Berkeley, and UC Santa Barbara. He was also the founding director of Nanoelectronics Research Facility at UCLA (established in 1989) with the infrastructure to further research in nanotechnology. His research interests include semiconductor nanodevices and nanotechnology; self-assembly growth of quantum structures and cooperative assembly of quantum-dot arrays; Si-based molecular beam epitaxy, quantum structures, and devices; nanoepitaxy of heterostructures; spintronics materials and devices; eand SiGe MBE and quantum structures. He holds 17 patents and has published over 300 papers.

Dr. Wang has received many awards, including the IBM Faculty Award; Guggenheim Fellowship; TSMC Honor Lectureship Award; Honoris Causa at Politechnico University, Torino, Italy; Semiconductor Research Corporation Inventor Award; and a Semiconductor Research Corporation Technical Excellence Achievement Award. He serves on the editorial board of the Encyclopedia of Nanoscience and Nanotechnology (New York: American Scientific). He is a Senior Editor for the IEEE TRANSACTIONS ON NANOTECHNOLOGY, and a Series Editor of Nanoscience and Nanotechnology for Artech House.

**Dongho Cha** received the B.S. degree in physics from Sungkyunkwan University, Korea, in 1990 and the M.S. degree in physics from Pohang University of Science and Technology (POSTECH), Korea, in 1995. He is currently working toward the Ph.D. degree in electrical engineering at the University of California, Los Angeles (UCLA).

From 1995 to 2002, he worked for Samsung Electronics as a Senior Engineer. His research interests include quantum dots, photo detectors, nanoelectronics, and optoelectronics.

**Jianlin Liu** received the B.S. and Ph.D. degrees in physics from Nanjing University, China, in 1993 and 1997, respectively, and another Ph.D. degree in electrical engineering from the University of California, Los Angeles (UCLA) in 2003.

In March 2003, Liu joined the Department of Electrical Engineering, University of California, Riverside, as a member of tenure-track faculty; currently he is an Assistant Professor. He has published three book chapters and more than 100 technical papers and conference proceedings. His areas of research interests include Si- and ZnO-based semiconductor materials growth, nanostructures fabrication, and nanodevices fabrication for applications in nanoelectronics and optoelectronics.

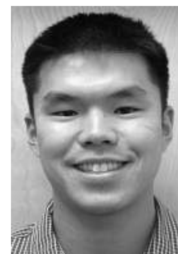

**Christopher Chen** received the B.S. degree in electrical engineering and computer sciences from University of California, Berkeley in 2004, and the M.S. degree in electrical engineering from University of California, Los Angeles in 2006. His M.S. thesis was on the development and characterization of Ge quantum dot infrared photodetectors.

In 2006, he joined the Modeling and Characterization Group at Altera Corporation (San Jose, CA) where he supports the development of MOSFET models for new FPGA products.